哈爾濱工業大學
HARBIN INSTITUTE OF TECHNOLOGY

High-temperature geopolymer & C_f reinforced composites and their derived CMC

Dechang Jia, Peigang He

Institute for Advanced Ceramics
Harbin Institute of Technology, Harbin, P.R. China

Saint-Quentin, France • July 4~6th, 2011

俄罗斯
哈萨克斯坦
阿斯塔纳
贝加尔湖
巴尔喀什湖
乌兰巴托
塔什干
比什凯克
吉尔吉斯斯坦
塔吉克斯坦
阿富汗
巴基斯坦
伊斯兰堡
新德里
印度
尼泊尔
加德满都
不丹
廷布
孟加拉国
达卡
缅甸
老挝
河内
越
万象
朝鲜
平壤
韩国
首尔(汉城)
日本
东京
黄海
东海
太平洋
琉球群岛
东沙群岛
巴布延群岛
吕宋岛
北回归线
新疆维吾尔自治区
乌鲁木齐
伊宁
吐鲁番
哈密
库尔勒
阿图什
和田
西藏自治区
拉萨
日喀则
珠穆朗玛峰 8844.43
噶尔
昌都
青海
西宁
格尔木
德令哈
玉树
甘肃
兰州
嘉峪关
金昌
宁夏回族自治区
银川
陕西
西安
庆阳
安康
四川
成都
马尔康
广元
达州
雅安
宜宾
西昌
重庆市
重庆
贵州
贵阳
遵义
云南
昆明
大理
丽江
曲靖
个旧
景洪
广西壮族自治区
南宁
桂林
贵港
北海
广东
广州
香港特别行政区
香港
澳门特别行政区
澳门
海南
海口
海南岛
湖南
长沙
张家界
衡阳
郴州
湖北
武汉
襄樊
江西
南昌
赣州
福建
福州
厦门
台湾
台北
澎湖列岛
台湾岛
钓鱼岛
赤尾屿
浙江
杭州
宁波
温州
舟山群岛
上海市
上海
江苏
南京
连云港
盐城
安徽
合肥
黄山
河南
郑州
信阳
安阳
山东
济南
青岛
烟台
东营
河北
石家庄
秦皇岛
北京
天津市
天津
山西
太原
朔州
内蒙古自治区
呼伦贝尔
锡林浩特
赤峰
辽宁
沈阳
丹东
长山群岛
吉林
长春
四平
延吉
松原
黑龙江
哈尔滨
齐齐哈尔
大庆
加格达奇
漠河
佳木斯

Three Locations in China

Where are we?

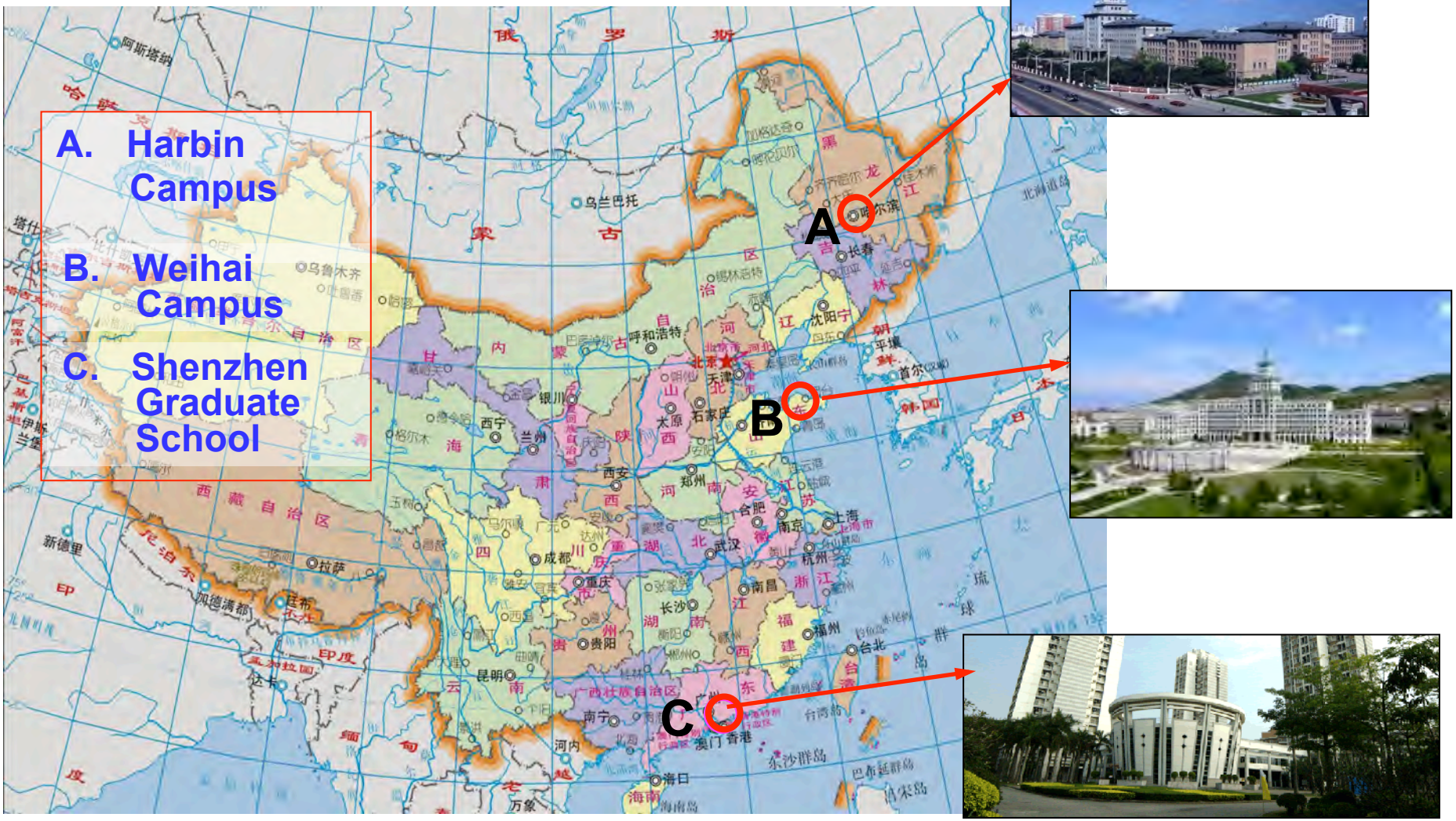

Three Locations in Harbin

A. Campus 1

B. Campus 2

C. Science Park

CONTENTS

1. Introduction

Geopolymer

Characteristics

- Environmental friendly
  —No CO_2 emission
- Low temperature fabrication
  —RT~150 ℃
- Ceramic formation ability upon heating
  —improved properties
- Adjustable thermal properties
  —Melting point、CTE

Applications and potential applications

- Geopolymer cement and concrete
- Refractory items
- Preparation of ceramics, i.e. Leucite
- Fireproof high-tech applications: aircraft interior, thermal insulators for racing car engine, etc. as an alternative to organic polymers

Low strength
brittleness
low reliability

→ **Geopolymer matrix composites** { particle / short fiber / continuous fiber

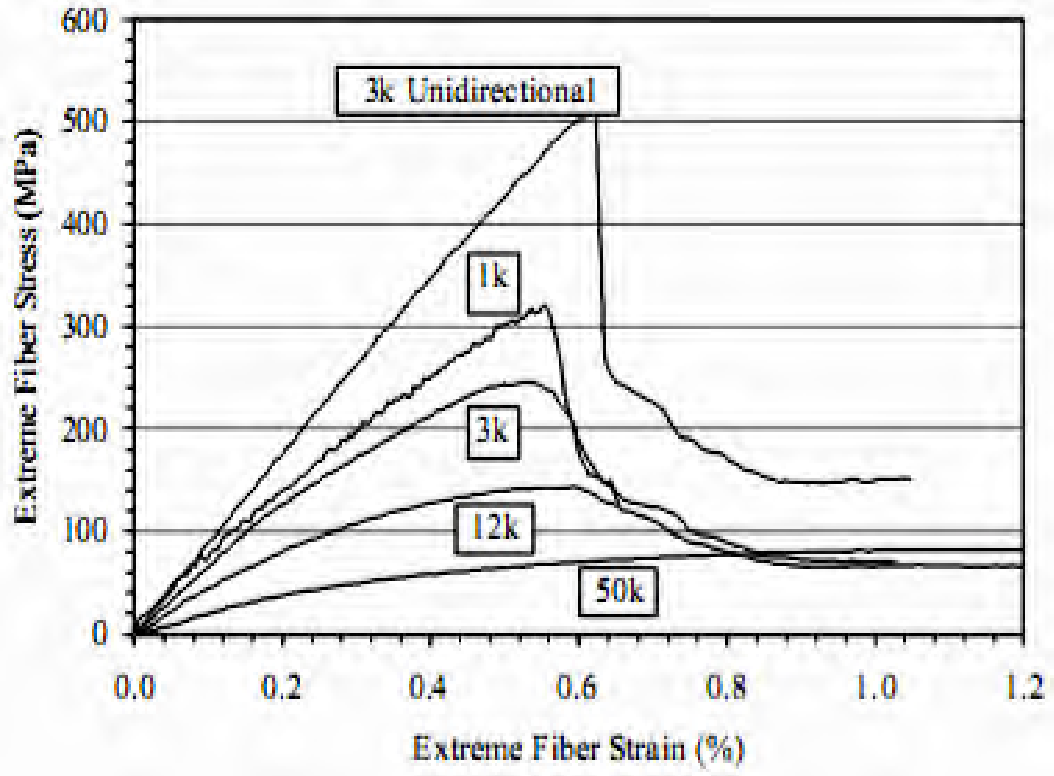

Fig.1 Stress-displacement curves of bidirectional carbon fiber reinforced geopolymer (Si/Al=27) composites. Fiber volume is 50%

---- J. Giancaspro, P. N. Balaguru, R. E. Lyon. *Proceedings of the Thirteenth International Offshore and Polar Engineering Conference*, Honolulu, Hawaoo, USA. 2003

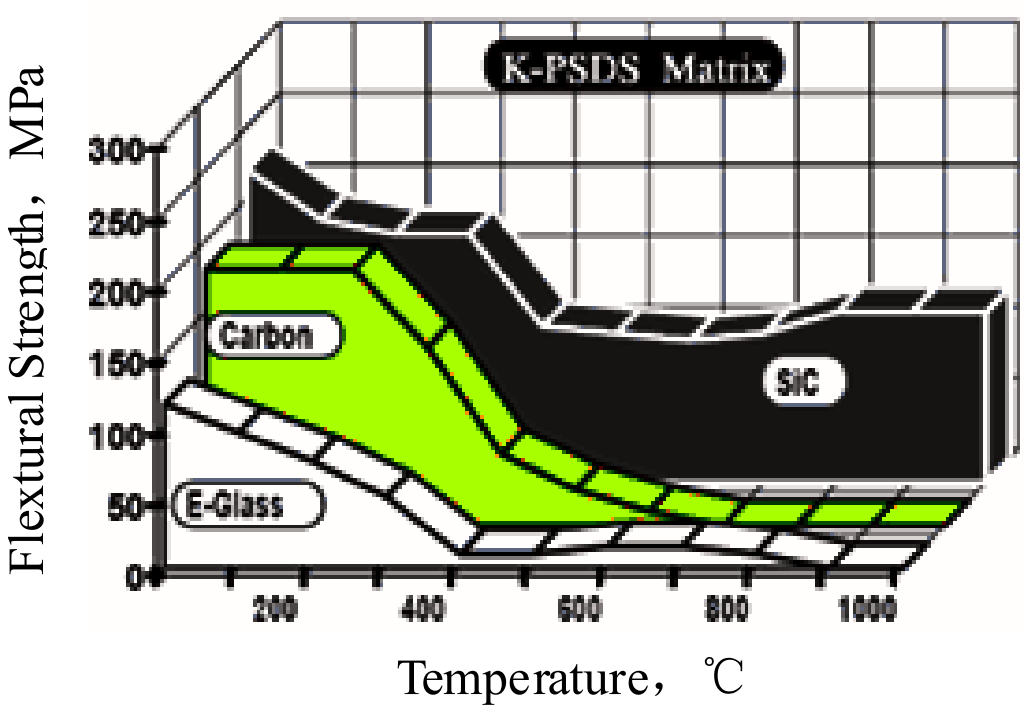

Fig.2 3-points flexural strength of geopolymer (Si/Al=3) composites reinforced by different kind of fibers (fiber contents is about 40vol%).

---- J. Davidovits, M. Davidovits. *36th Annual SAMPE Symposium*, 1991, 1939~1949

2. Thermal evolution and crystallization of geopolymer

2.1 Thermal evolution and crystallization mechanism of KGP

2.2 Effect of Cesium substitution on the crystallization of geopolymer

2.3 Effects of Cesium substitution on the phase transition of leucite

2.1 Thermal evolution and crystallization of KGP

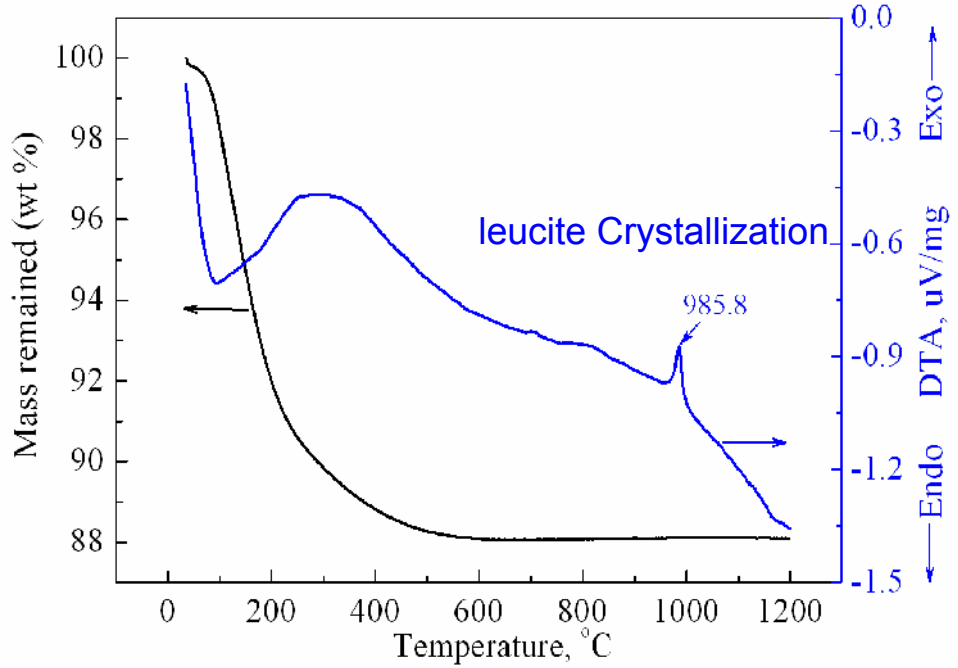

Fig.2-1 TG/DTA of KGP

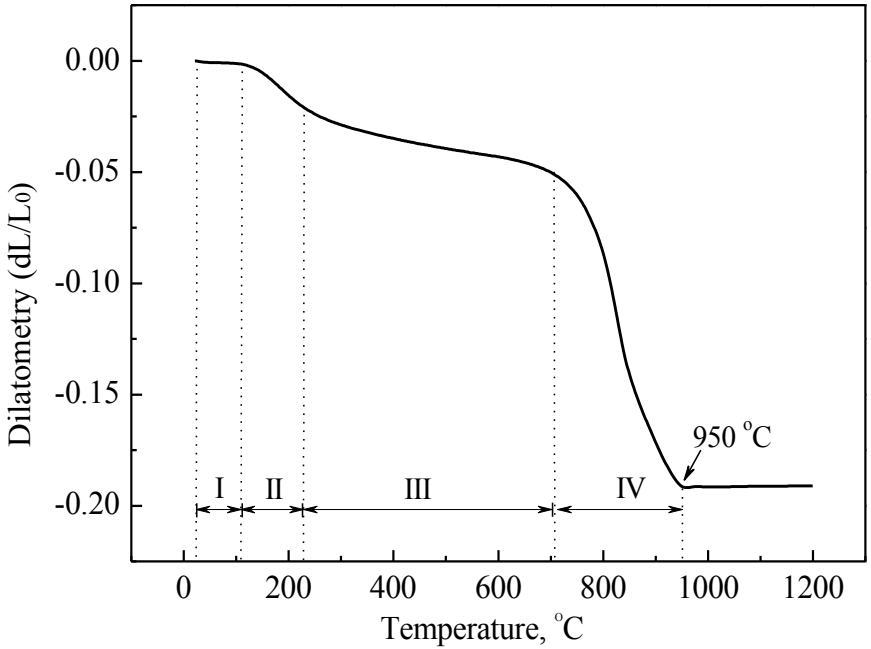

Fig.2-2 Thermal shrinkage of KGP

---- Peigang He, Dechang Jia. *Ceramics International*. 2011, 37 (1), 59-63.

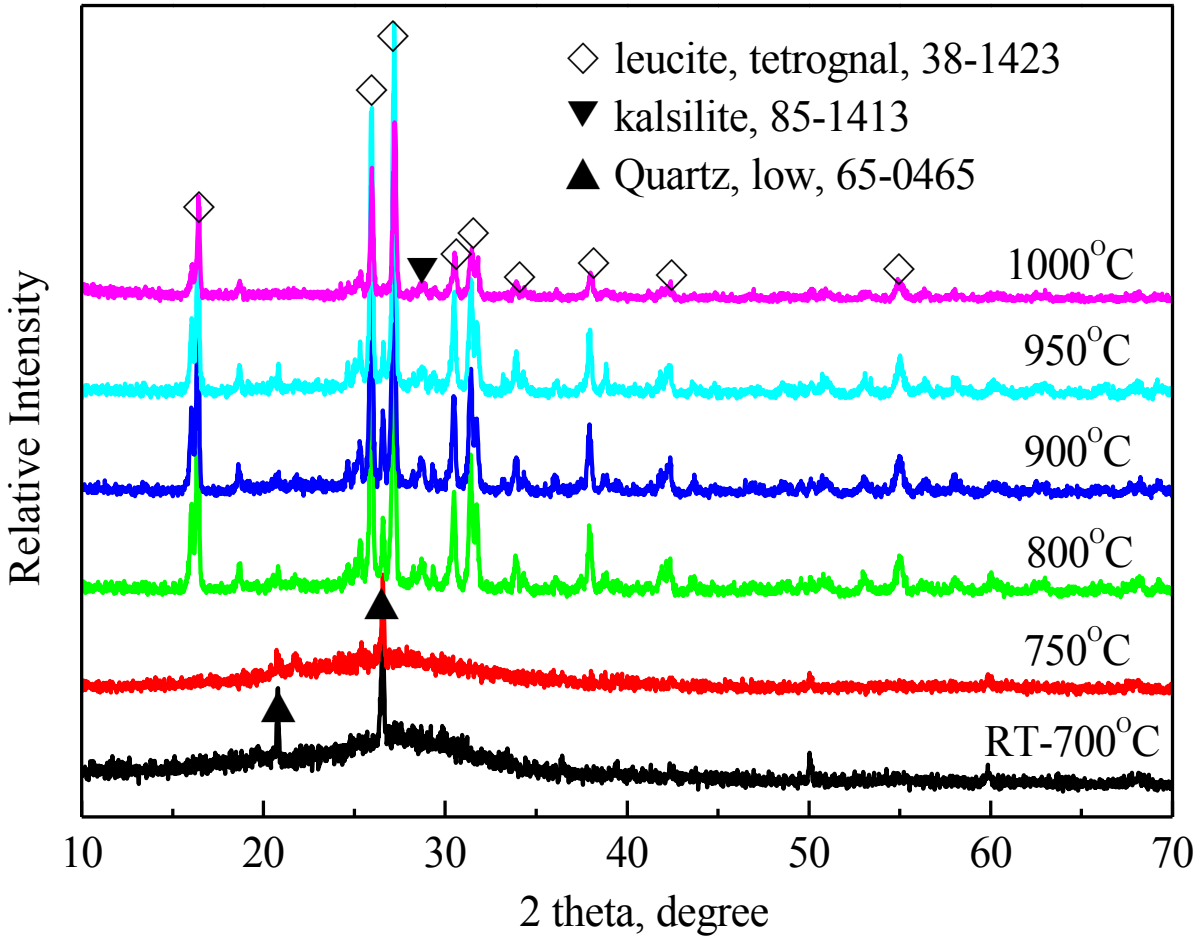

Fig.2-3 XRD pattern of KGP soaked at different temperature for 2h

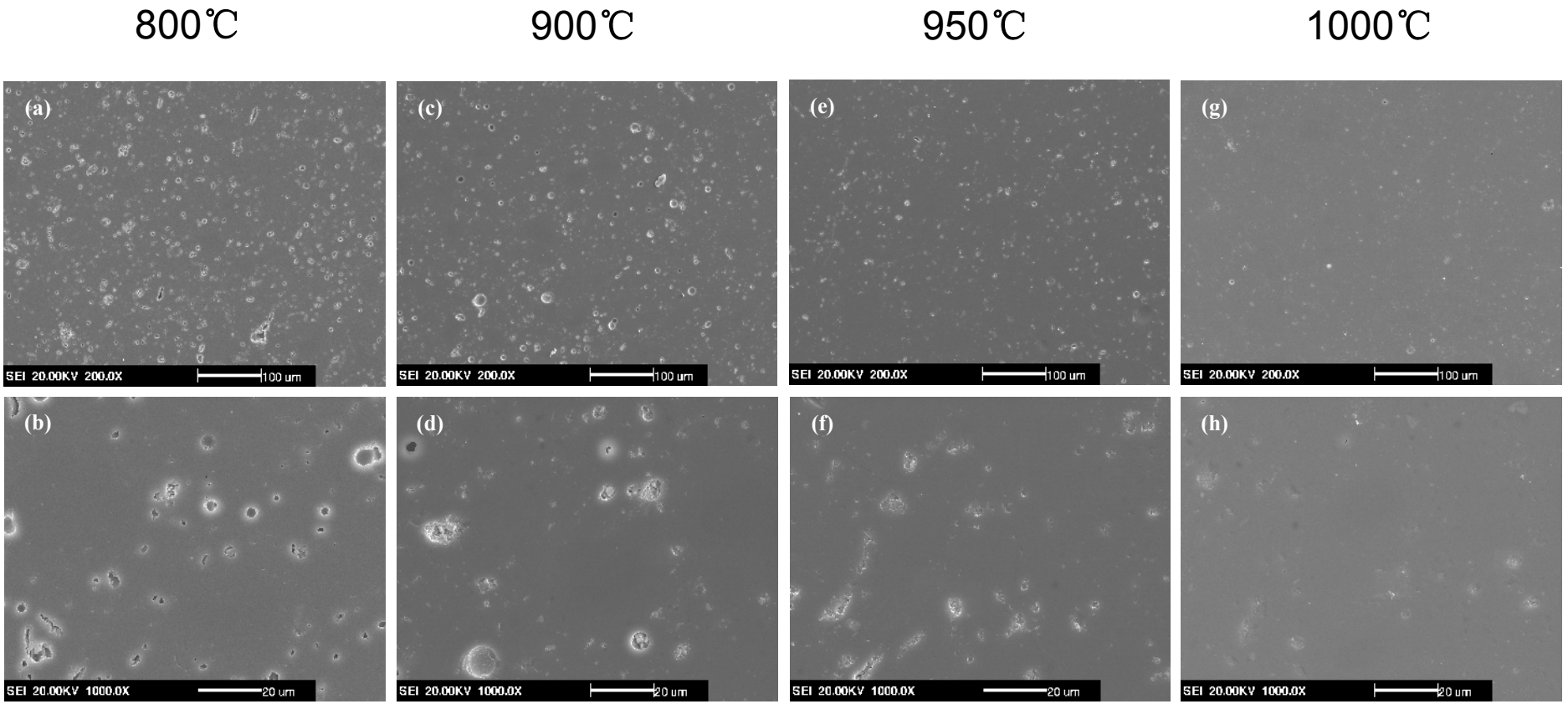

Fig.2-4 Microstructure of KGP soaked at different temperature for 2h. (a), (b) 800℃; (c), (d) 900℃; (e), (f) 950℃; (g), (h) 1000℃.

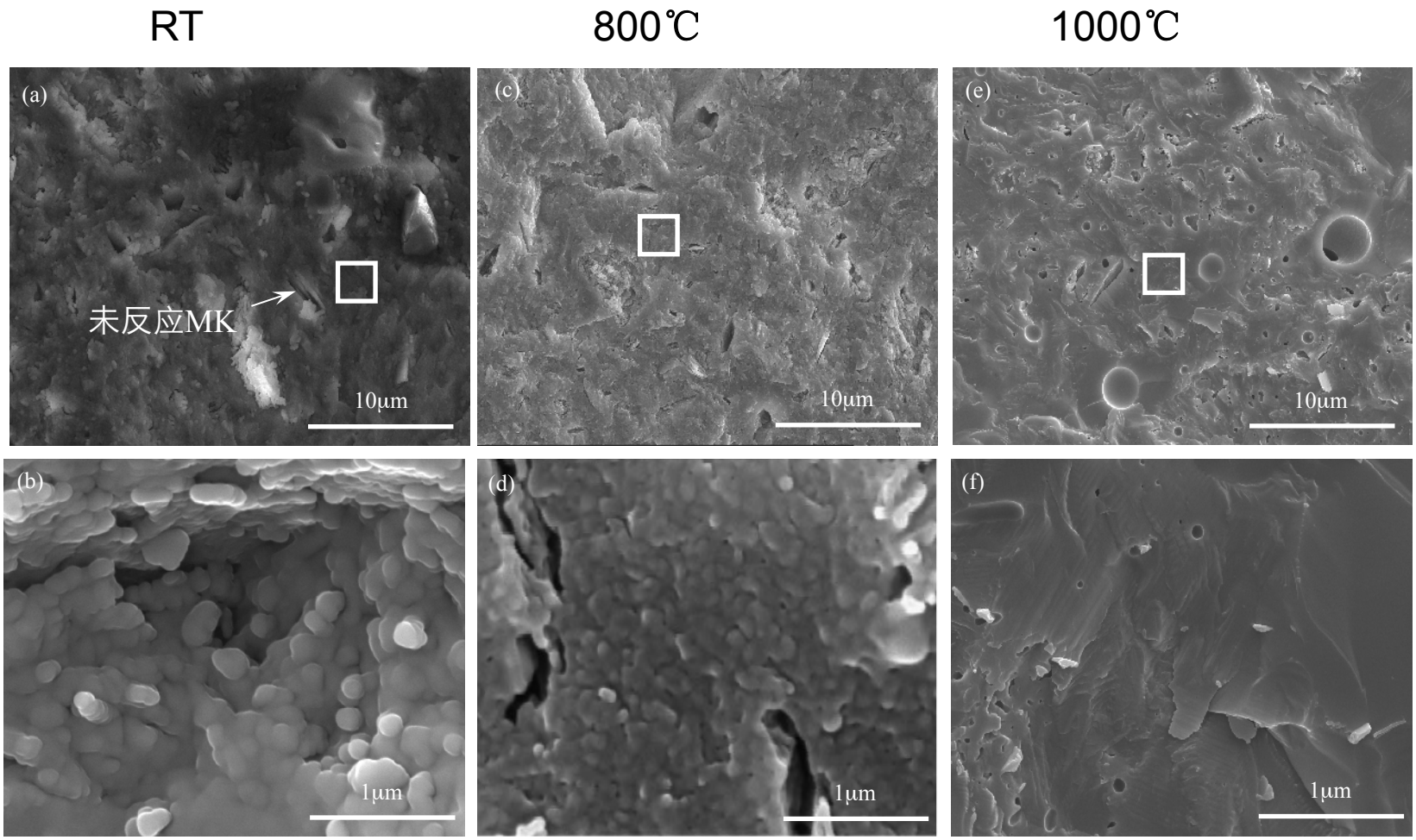

Fig.2-5 Fractographs of KGP soaked at different temperature for 2h
(a), (b) RT; (c), (d) 800℃; (e), (f) 1000℃

---- Peigang He, Dechang Jia. *Ceramics International*. 2011, 37 (1), 59-63.

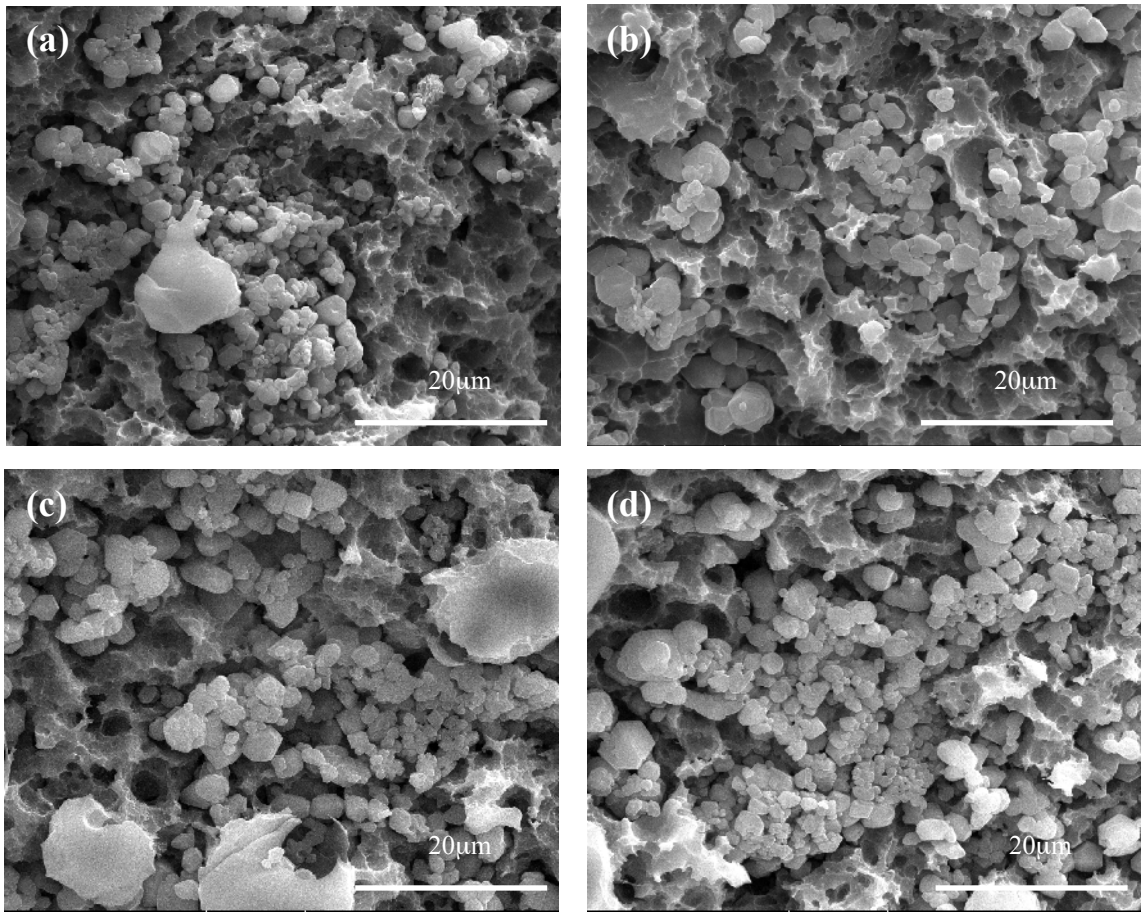

Fig.2-6 Fracture surface morphology of the KGP treated at different temperature and etched in 3wt.% HF at room temperature for 30s: (a) 800℃, (b) 900℃, (c) 950℃, (d) 1000℃

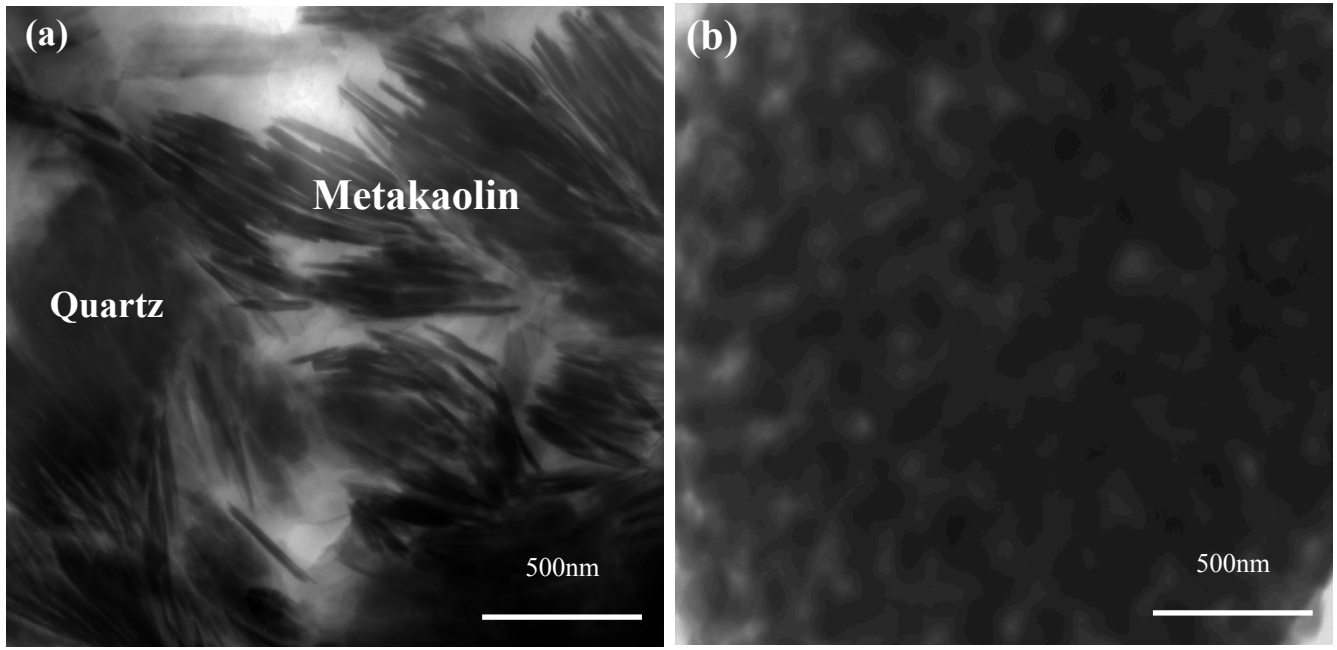

Fig.2-7 TEM images of: metakaolin (a) and the resulted geopolymer (b)

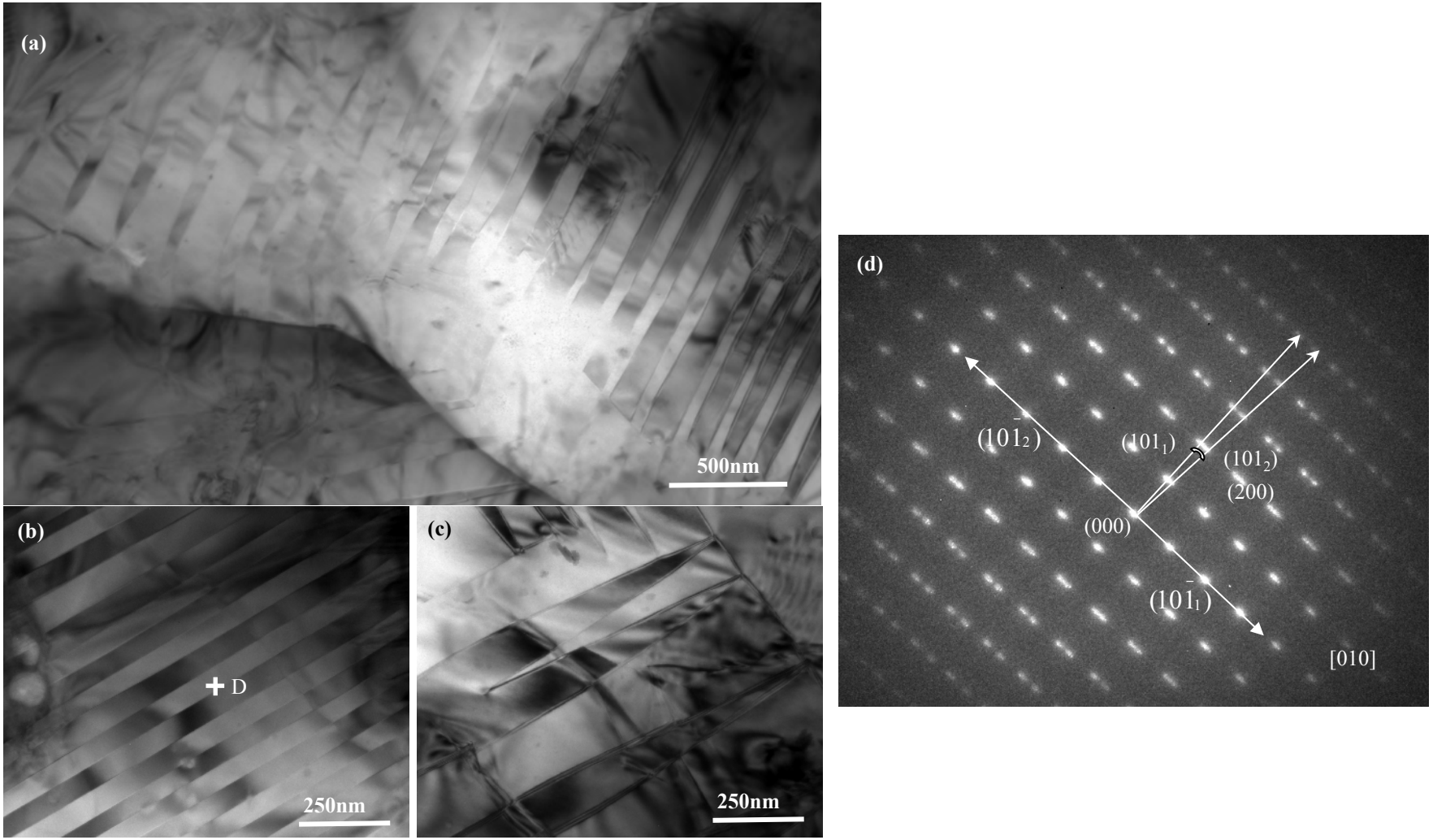

Fig. 2-8 TEM observation of geopolymer treated at 1000℃ for 2h:
(a) low magnification, (b) and (c) high magnification, (d) SAD pattern of area D

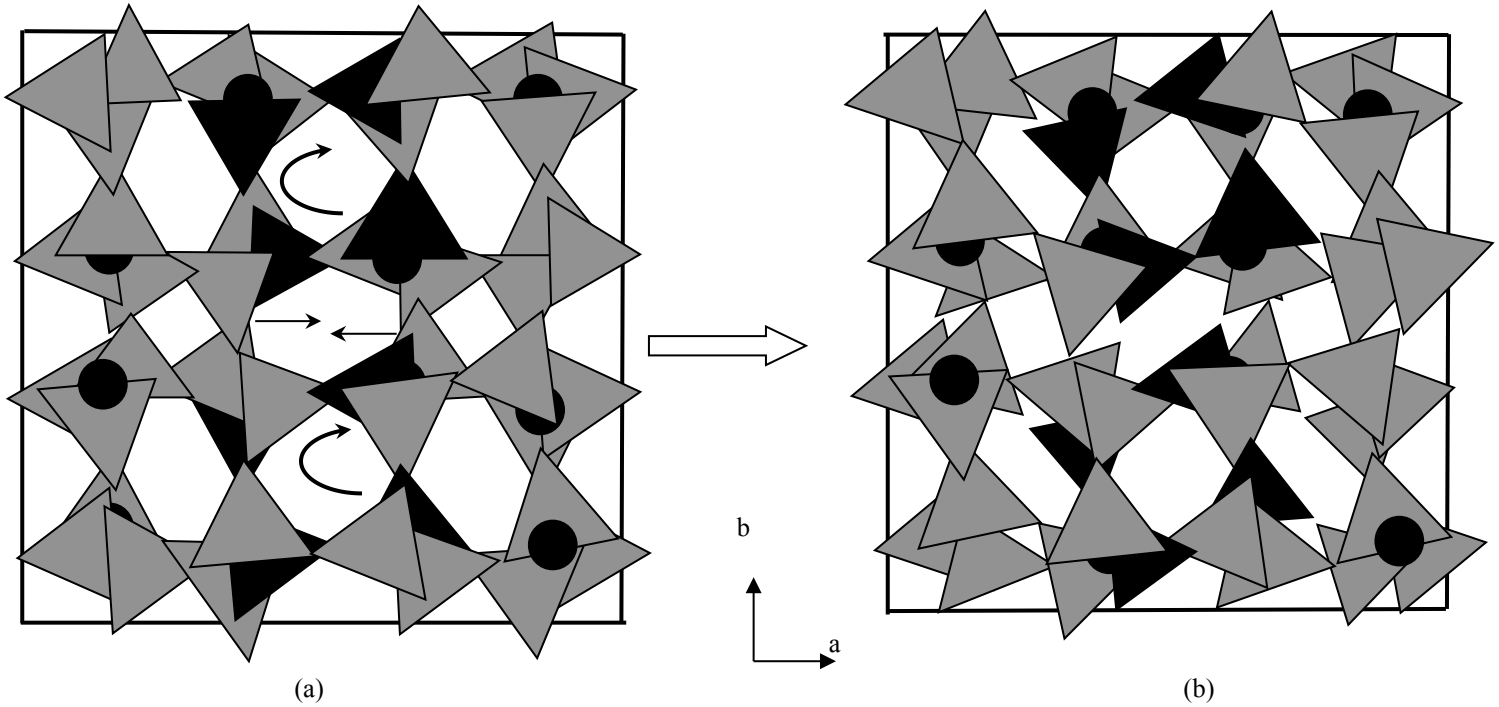

Fig. 2-9 Crystal structures of leucite: (a) cubic phase, (b) tetrahedral phase

△ : $Al(Si)O_4$

● : K

Black tetrahedron : The fourfold rings

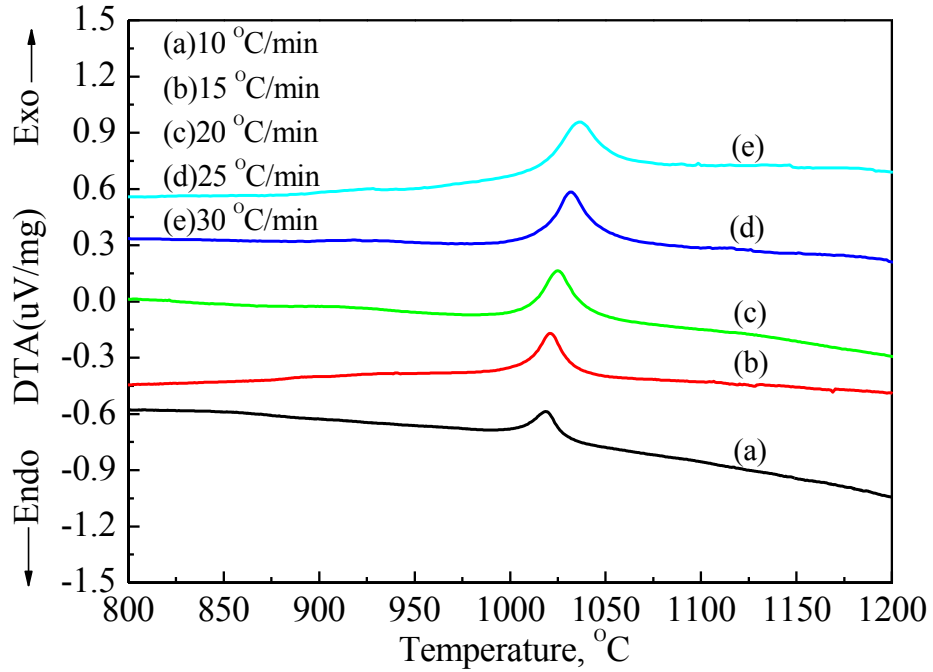

Fig. 2-10 DTA of KGP using different heating rates

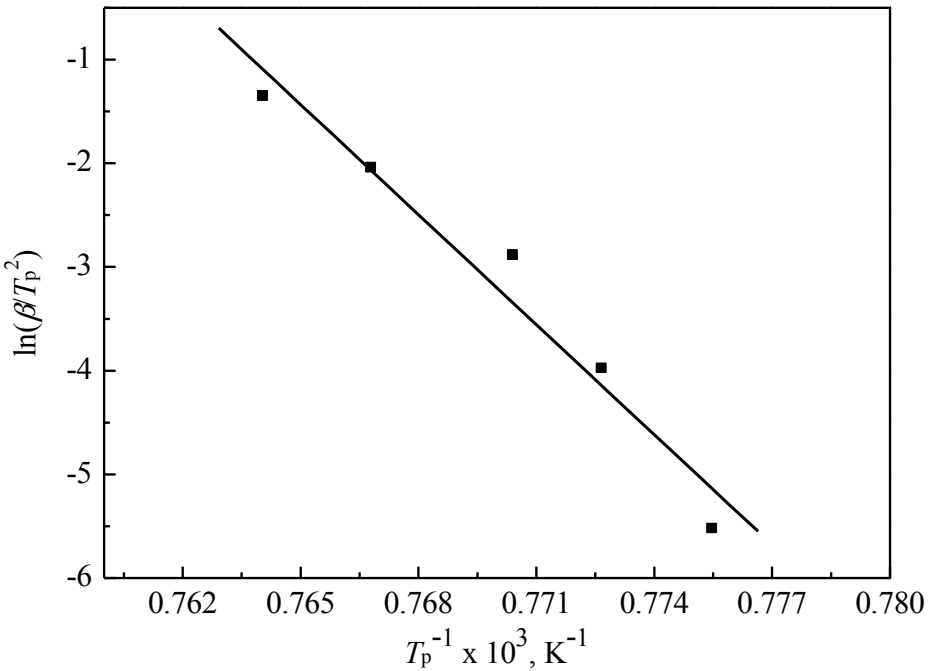

Fig. 2-11 Kissinger plot of $\ln(\beta/T_p^2)$ vs. T_p^{-1}

Kissinger method: $$\ln\left(\frac{T_p^2}{\beta}\right) = -\frac{E_c}{RT_p} + \ln\frac{E}{R\upsilon}$$

Augis-Bennett: $$n = \frac{2.5RT_p^2}{\Delta TE}$$

n=3.89, Ea=455.9 kJ/mol

Three dimensional crystal growth mechanism

---- Peigang He, Dechang Jia. *Ceramics International*. 2011, 37 (1), 59-63.

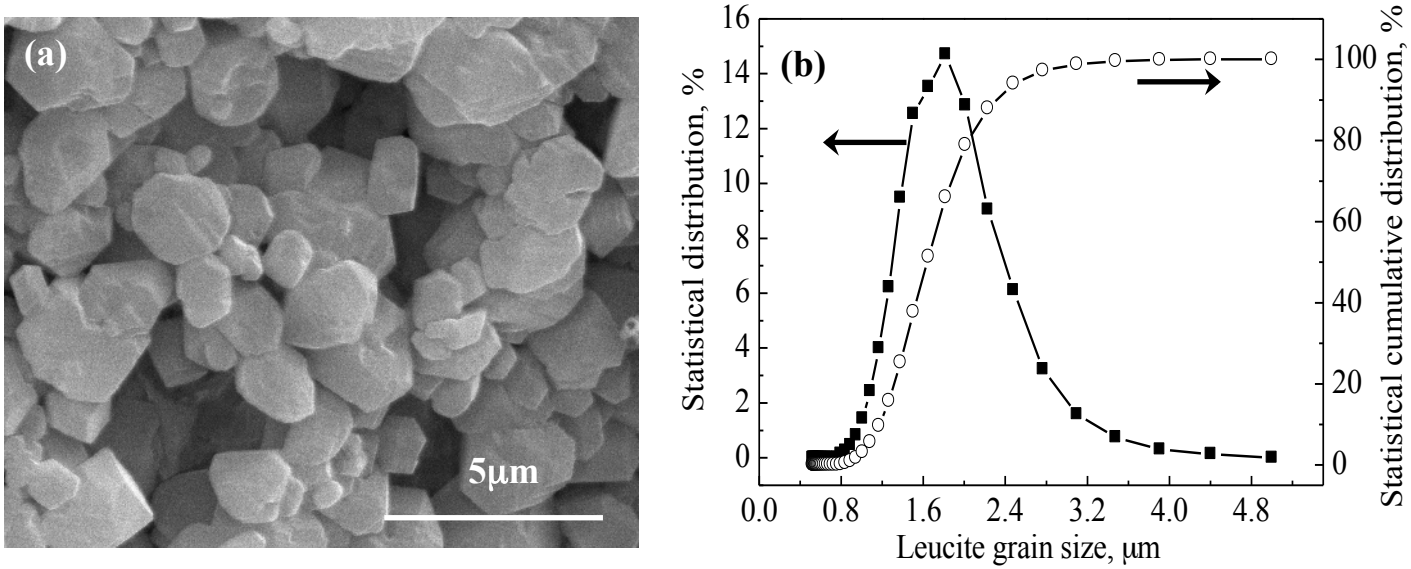

Fig. 2-12 SEM micrographs of leucite grains (a) and size distribution (b)

Table 2-1 Mechanical properties of the geopolymer and the resulted leucite ceramic

Specimen	Flexural strength (MPa)	Young's modulus (GPa)	Fracture toughness (MPa · $m^{1/2}$)	Vickers hardness (GPa)
KGP	12.3±1.2	10.3±1.2	0.2±0.04	0.68±0.04
Leucite ceramic	70.0±6.8	65.0±6.3	1.3±0.16	7.39±0.24

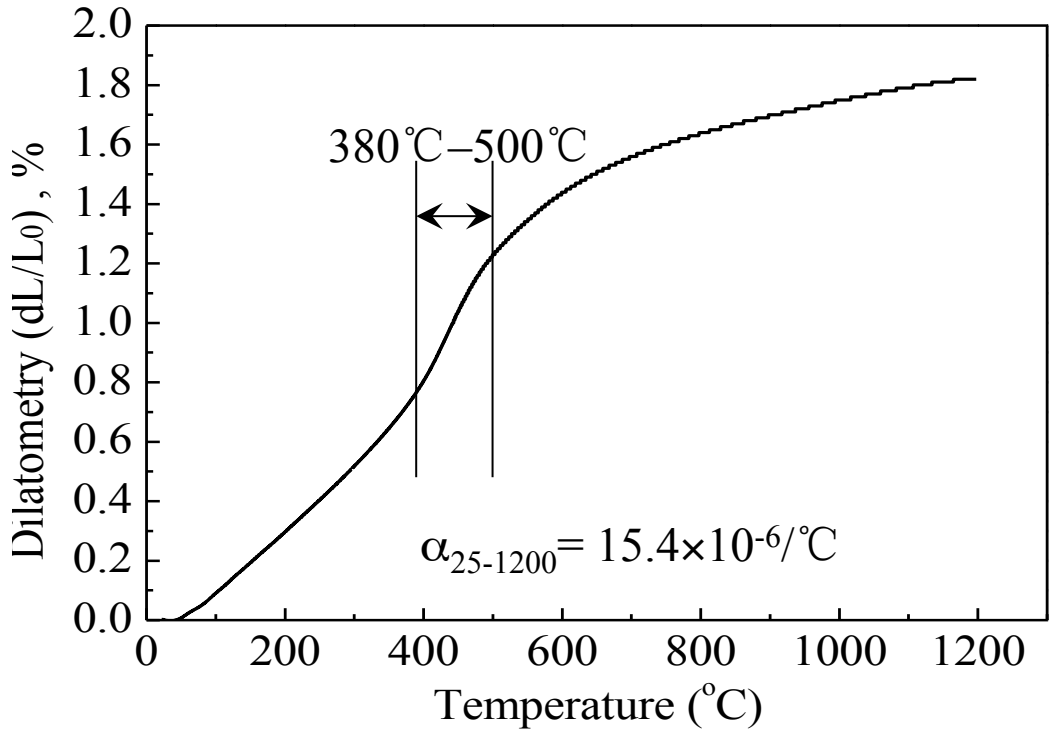

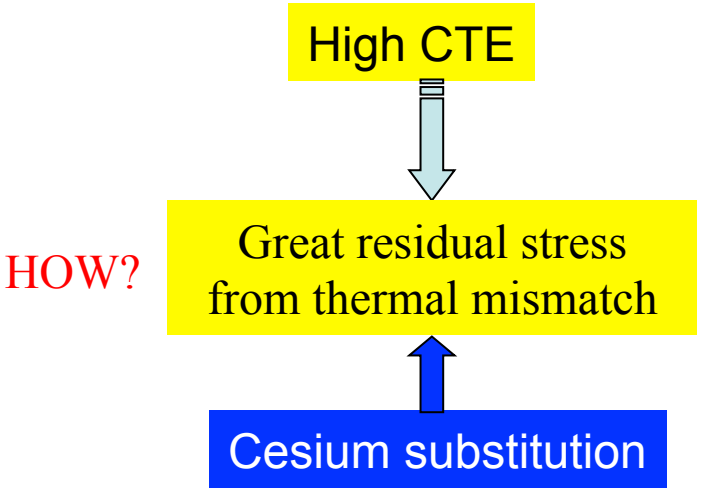

Fig.2-13 Thermal expansion of the ceramics derived from KGP

2.2 Effect of Cesium substitution on the crystallization of geopolymer

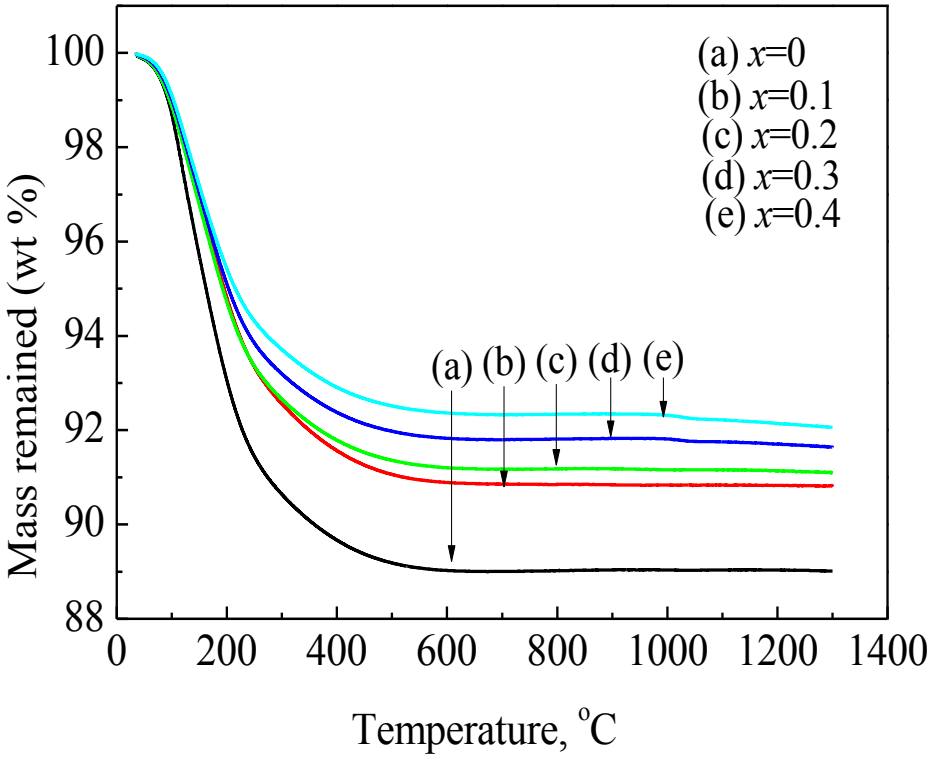

Fig. 2-14 Weight loss of $Cs_xK_{(1-x)}GP$

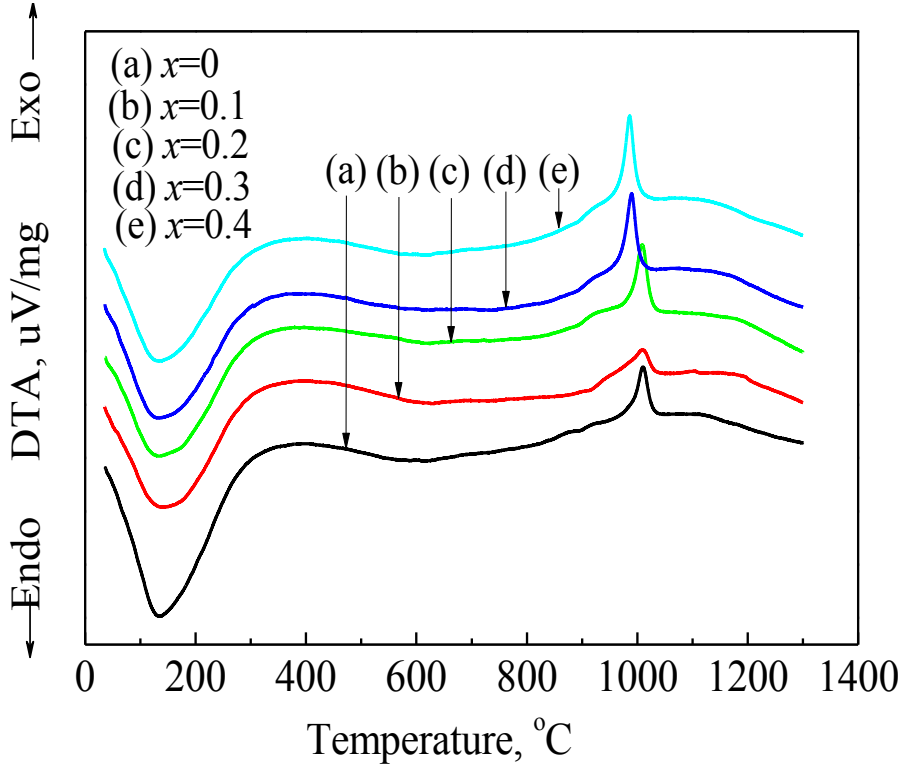

Fig. 2-15 DTA of $Cs_xK_{(1-x)}GP$

---- Peigang He, Dechang Jia. *Ceramics International*. 2010, 36 (8), 2395-2400.

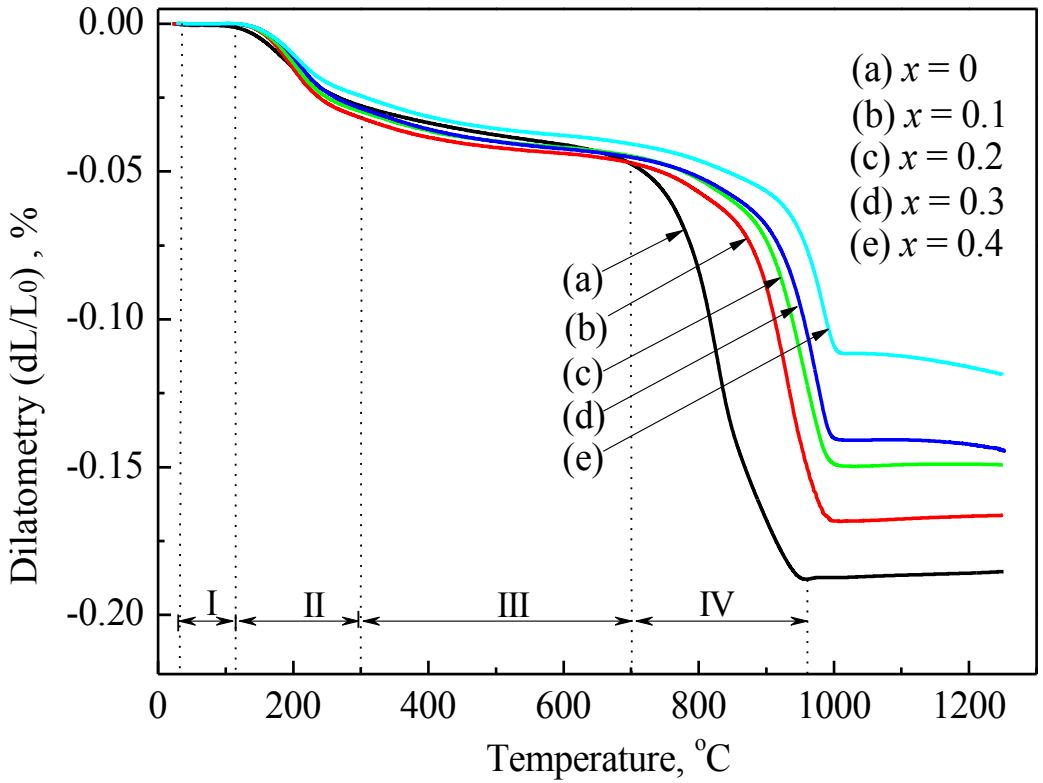

Fig.2-16 Thermal shrinkage of $Cs_xK_{(1-x)}GP$

---- Peigang He, Dechang Jia. *Ceramics International*. 2010, 36 (8), 2395-2400.

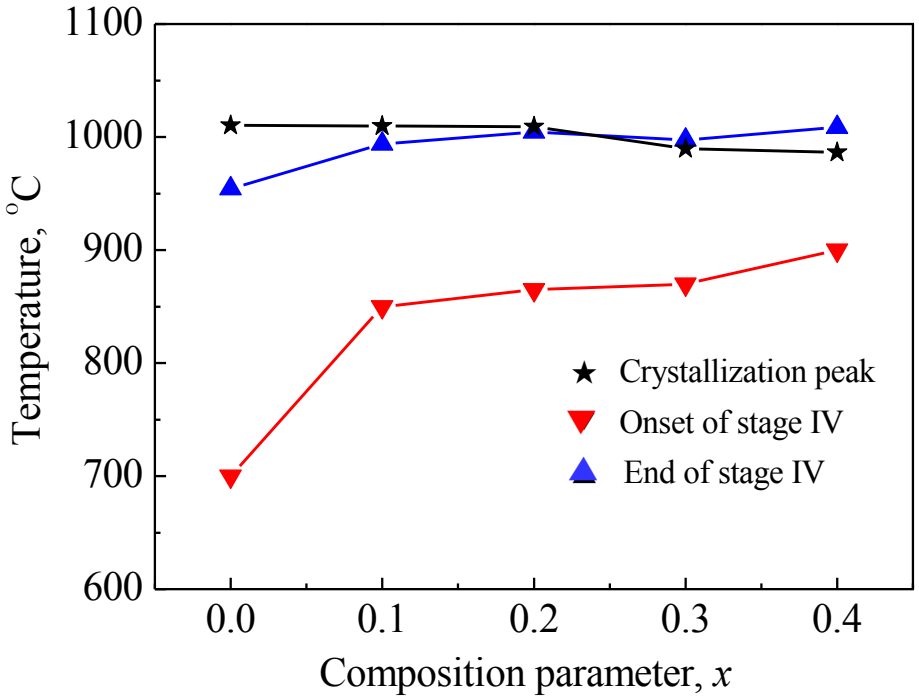

Fig. 2-17 Onset and end temperature of stage IV and crystallization temperature of $Cs_xK_{(1-x)}GP$

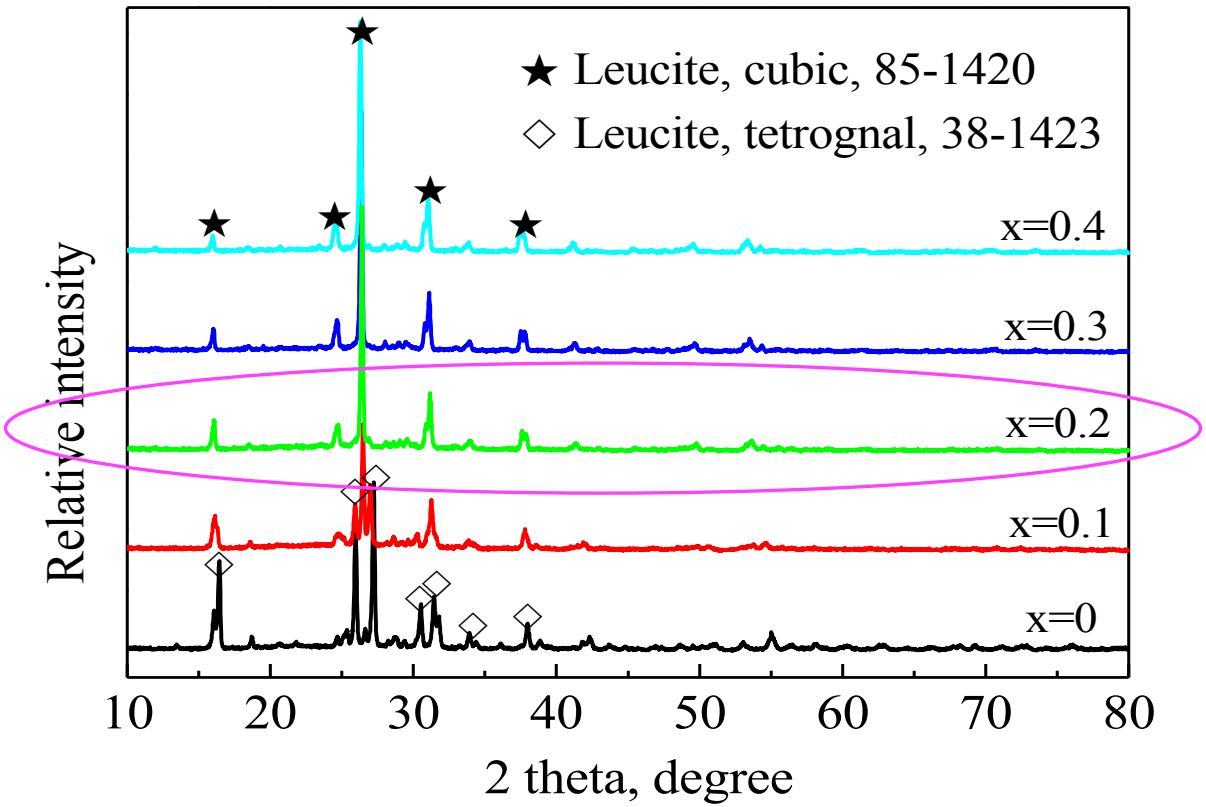

Fig. 2-18 XRD patterns of $Cs_xK_{(1-x)}GP$ ceramics heat treated at 1200℃ for 2h

---- Peigang He, Dechang Jia. *Ceramics International*. 2010, 36 (8), 2395-2400.

2.3 Effects of Cesium substitution on the phase transition of leucite

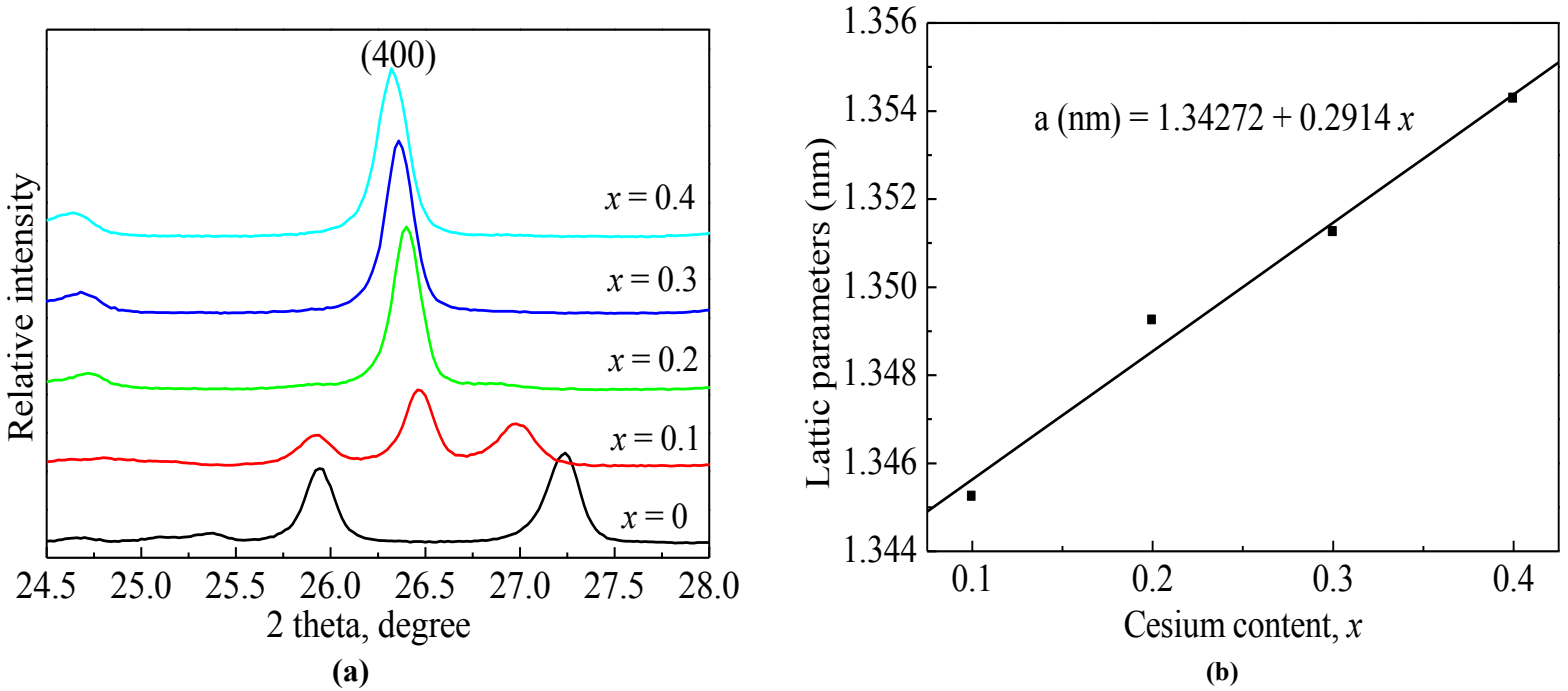

Fig. 2-19 Slow step-scan XRD patterns in a 2θ range of 24.5~28° (a) and the calculated lattice parameters (b) of leucite

---- Peigang He, Dechang Jia. *Ceramics International*. 2010, 36 (8), 2395-2400.

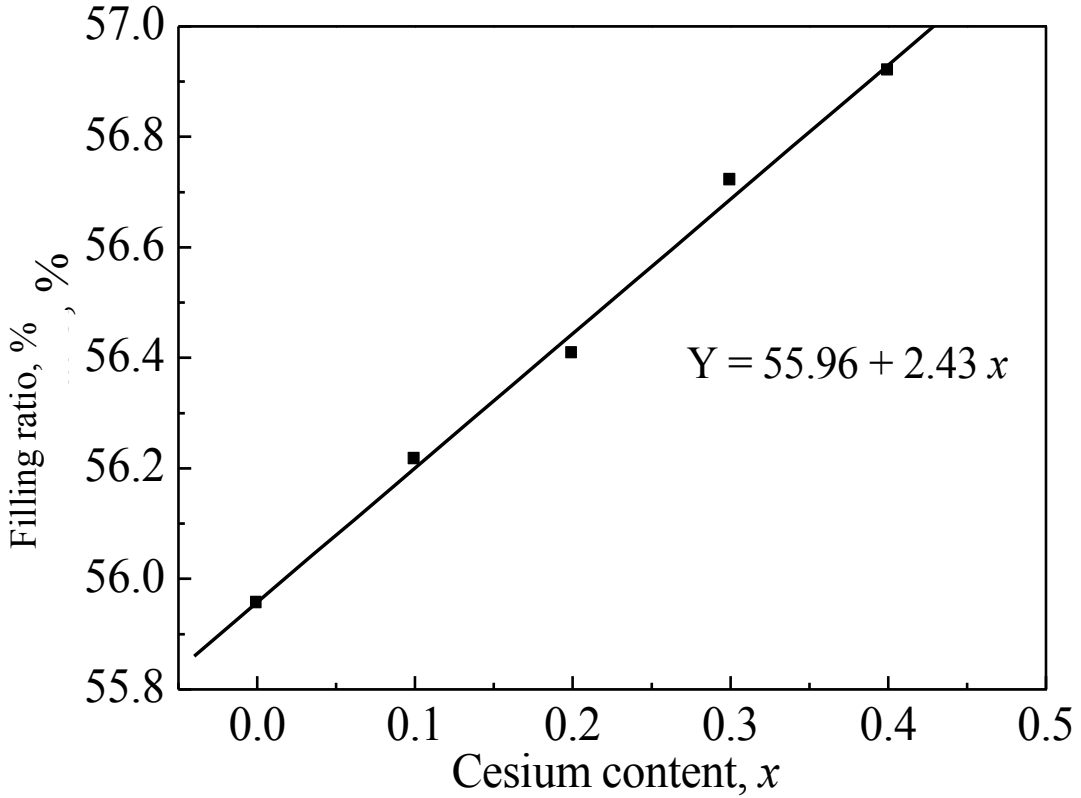

Fig. 2-20 The filling ratio of leucite crystal cell derived from $Cs_xK_{(1-x)}GP$

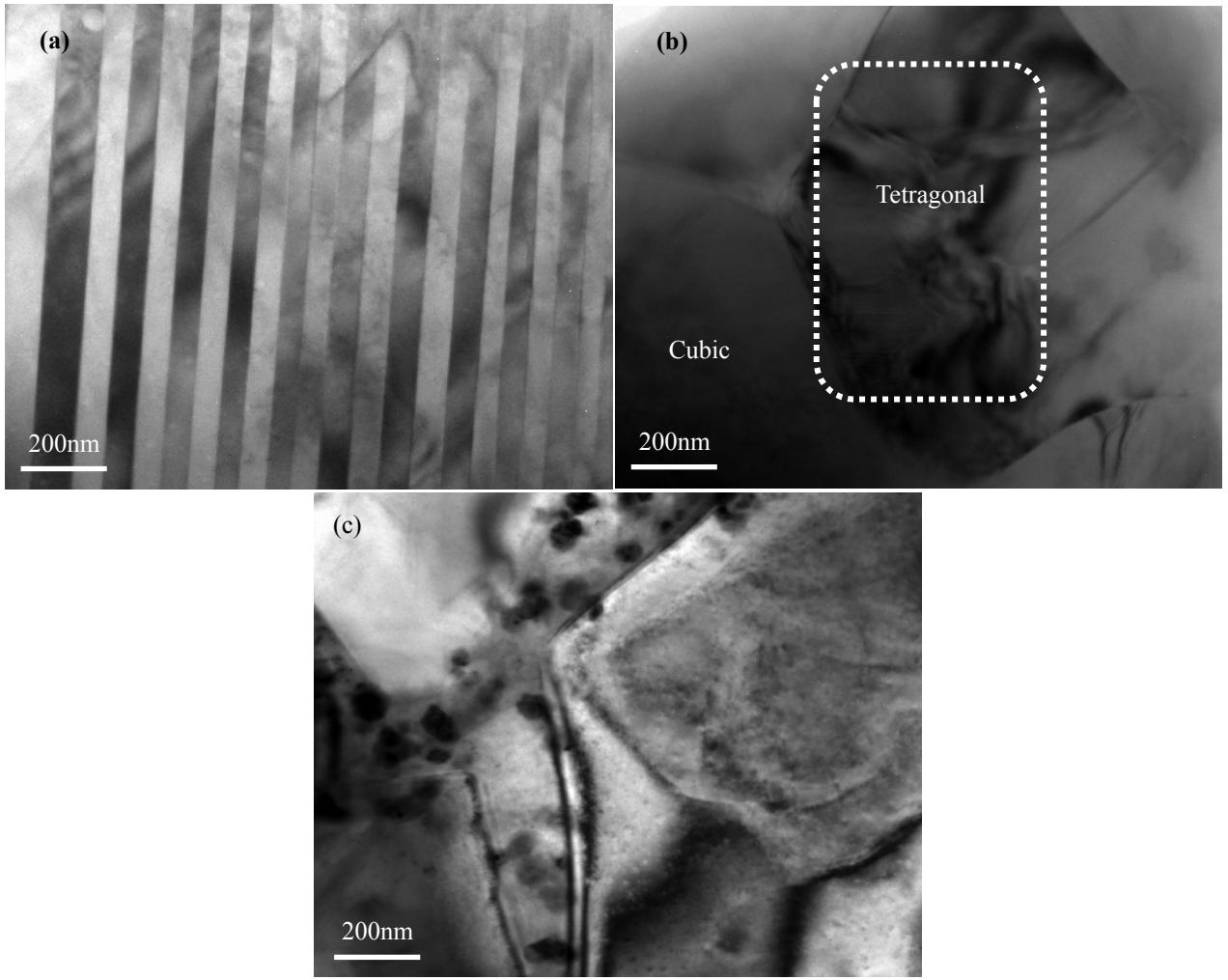

Fig. 2-21 TEM micrographs of the ceramics derived from $Cs_xK_{(1-x)}GP$: (a) x=0, (b) x=0.1, (c) x=0.2.

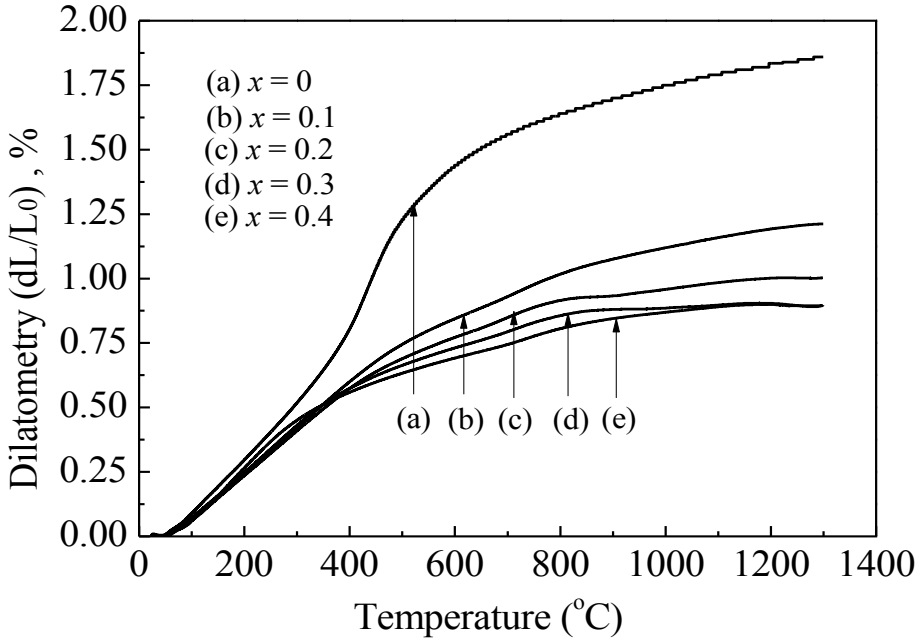

Fig. 2-22 Thermal expansion curves of $Cs_xK_{(1-x)}GP$ ceramic

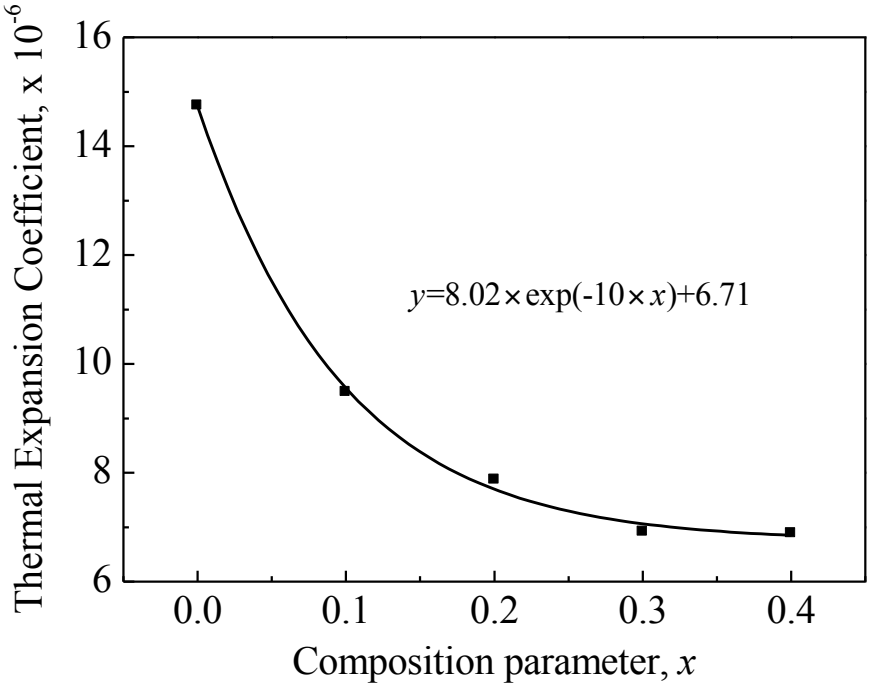

Fig. 2-23 Linear coefficient of thermal expansion of $Cs_xK_{(1-x)}GP$ ceramic

---- Peigang He, Dechang Jia. *Ceramics International*. 2010, 36 (8), 2395-2400.

2.4 Summary

- Geopolymer technology provides a novel method to fabricate leucite ceramic with greatly improved mechanical properties.
- Thermal shrinkage of geopolymer during heat treatment can be divided into structural resilience, dehydration, dehydroxylation and sintering.
- For the K-based geopolymer, leucite crystallization appeared after the sintering stage and the Avarami parameter indicates the three-dimensional crystal growth mechanism.
- Leucite ceramic posses an adjustable thermal expansion coefficient by doping cesium ions.

3. Effects of high-temperature heat treatment on the mechanical properties of C_f/geopolymer composites

3.1 Effects of heat treatment on the properties of C_f/KGP

3.2 Effects of heat treatment on the mechanical properties of C_f/CsKGP

3.3 Summary

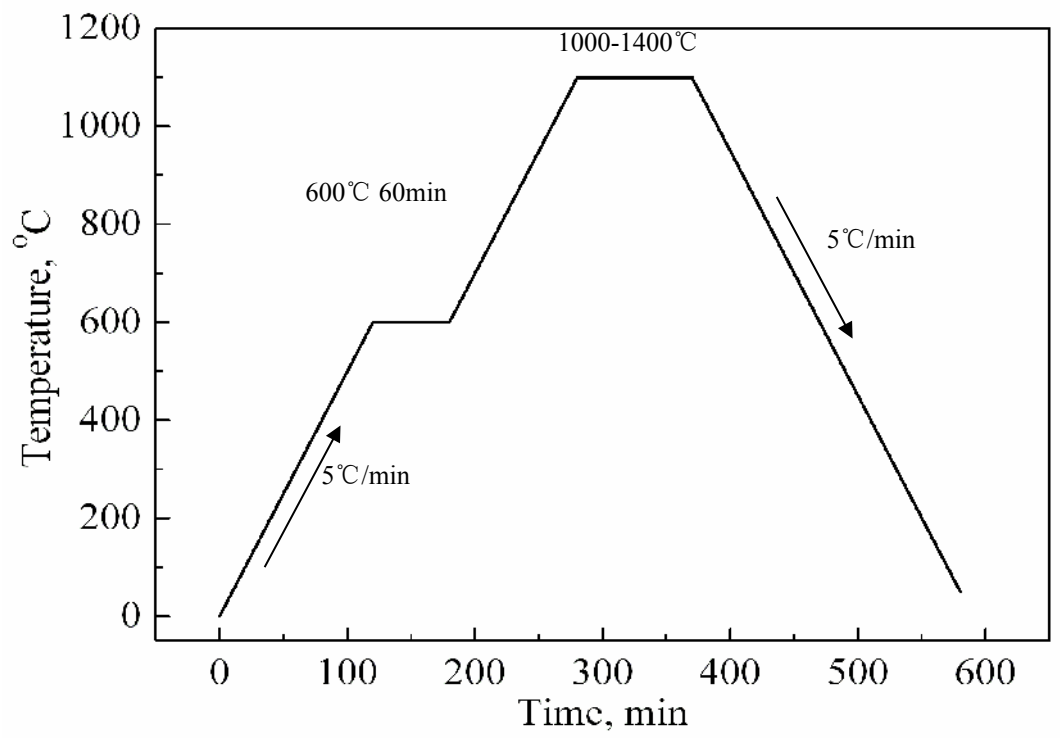

Fig. 3-1 High-temperature heat treatment procedure of the composites

3.1 Effects of heat treatment on the properties of C_f/KGP

- **Carbon fiber**: Unidirectional
- **Matrix**: $K_2O \cdot Al_2O_3 \cdot (3 \sim 5)SiO_2 \cdot 11H_2O$
- **Composites without and after heat treatment were denoted as:**

  KC-W, KC-1000, KC-1100, KC-1200, KC-1300 and KC-1400, respectively
- **Fiber contents**: 20vol% for KC-W and 25vol% for others

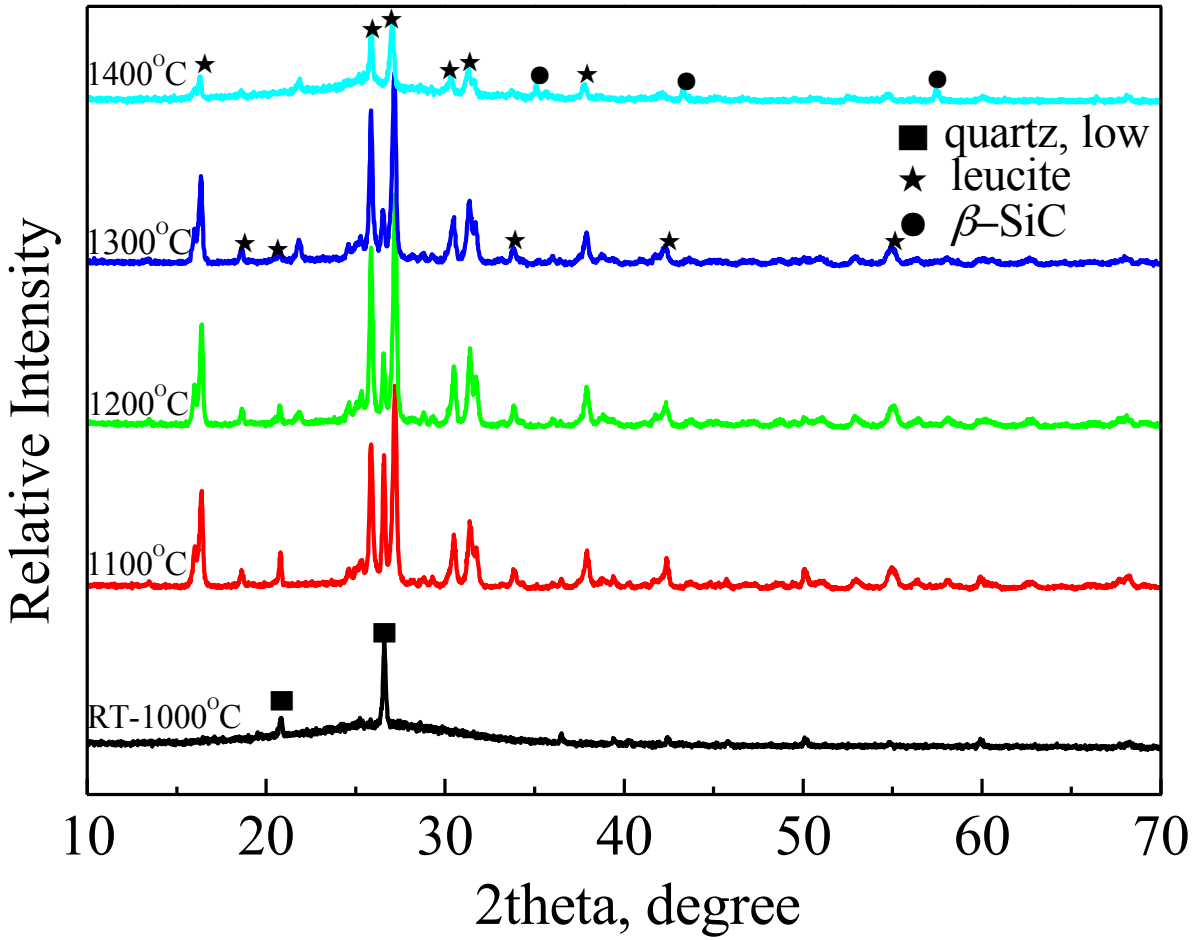

Fig. 3-2 XRD patterns of C_f/KGP heat treated at different temperature

---- Peigang He, Dechang Jia. *Ceramics International*. 2010, 36 (4), 1447-1453.

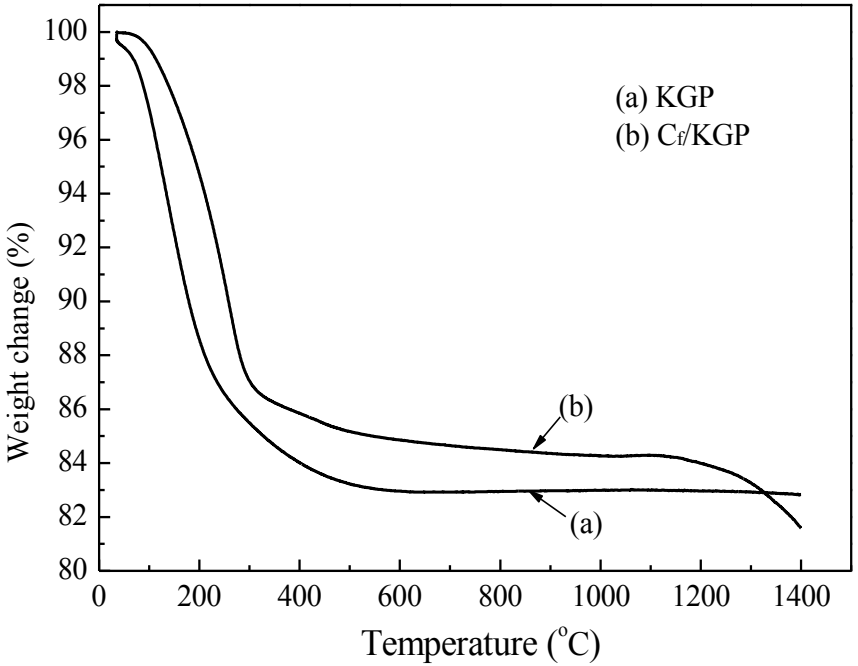

Fig. 3-3 Weight loss of KGP and C_f/KGP

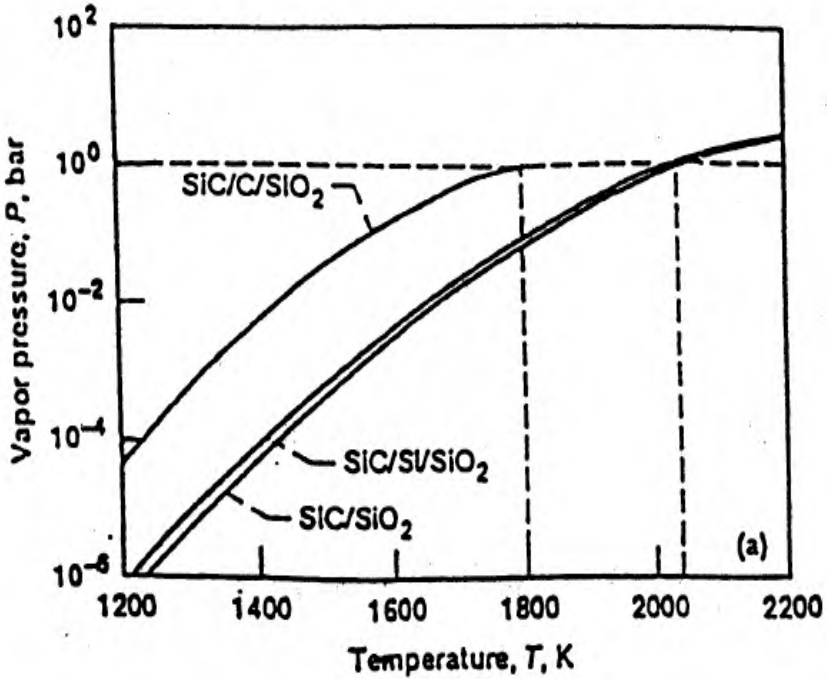

Fig. 3-4 Total vapor pressure of interfacial reaction of Si–C–O system as a function of temperature [32]

$$Si\text{-}O + C \longrightarrow SiC + CO(g) \qquad (3\text{-}1)$$

---- Peigang He, Dechang Jia. *Ceramics International*. 2010, 36 (4), 1447-1453.

Table 3-1 The reactions and standard Gibbs free energy

Reaction	Standard Gibbs free energy ($J \cdot mol^{-1}$)
(1) $C_{(s)} + 0.5O_{2(g)} = CO_{(g)}$	$-114400-85.77T$
(2) $Si_{(s)}+C_{(s)} = SiC_{(s)}$	$-73050+7.66T$
(3) $Si_{(s)}+O_{2(g)} = SiO_{2(s)}$	$-907100+175.73T$

Gibbs free energy for (3-1)： $\Delta G^\circ = 605250 - 339.61T$

The theoretical reaction temperature is 1782℃

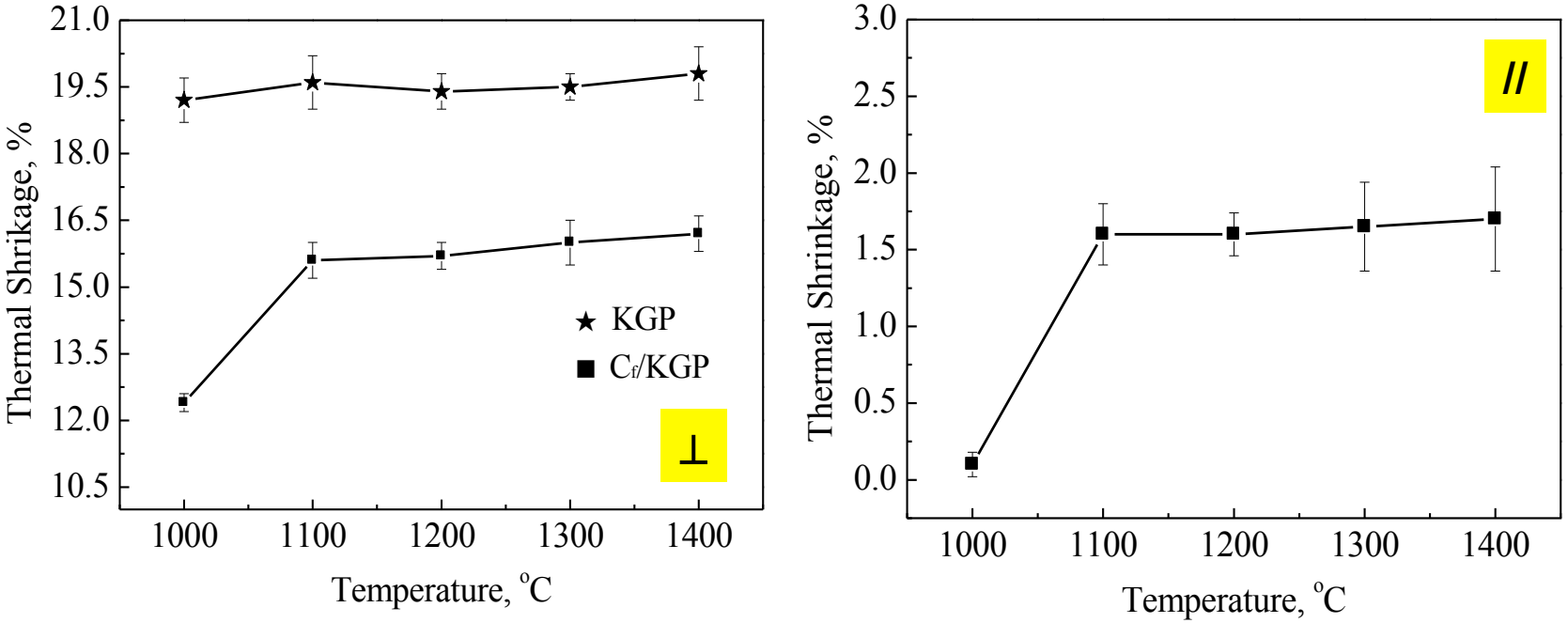

Fig. 3-5 Thermal shrinkages of the composite heat treated in different directions: (a) perpendicular and (b) parallel to the fiber direction

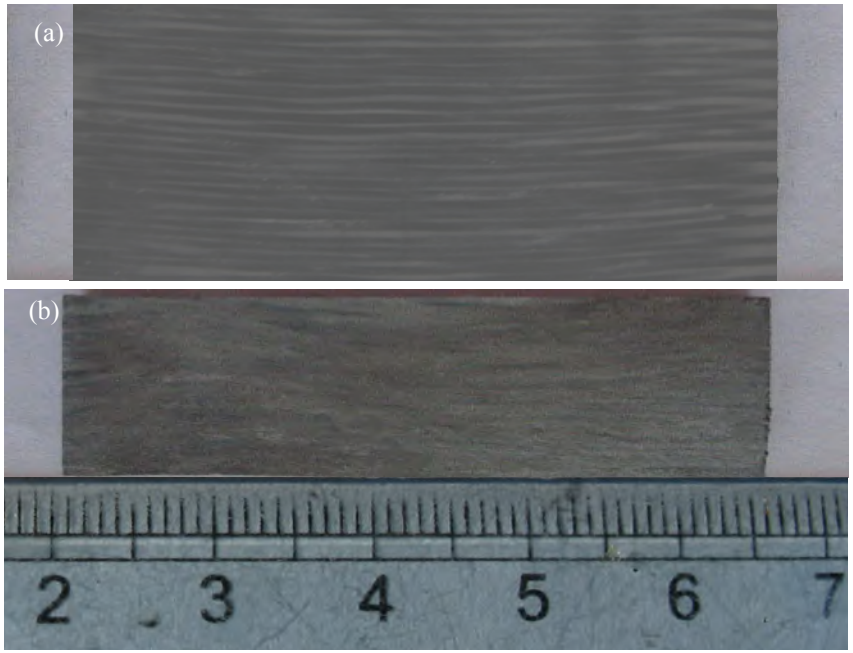

Fig. 3-6 Morphologies of C_f/KGP composite (a) before and (b) after heat treatment at 1100℃

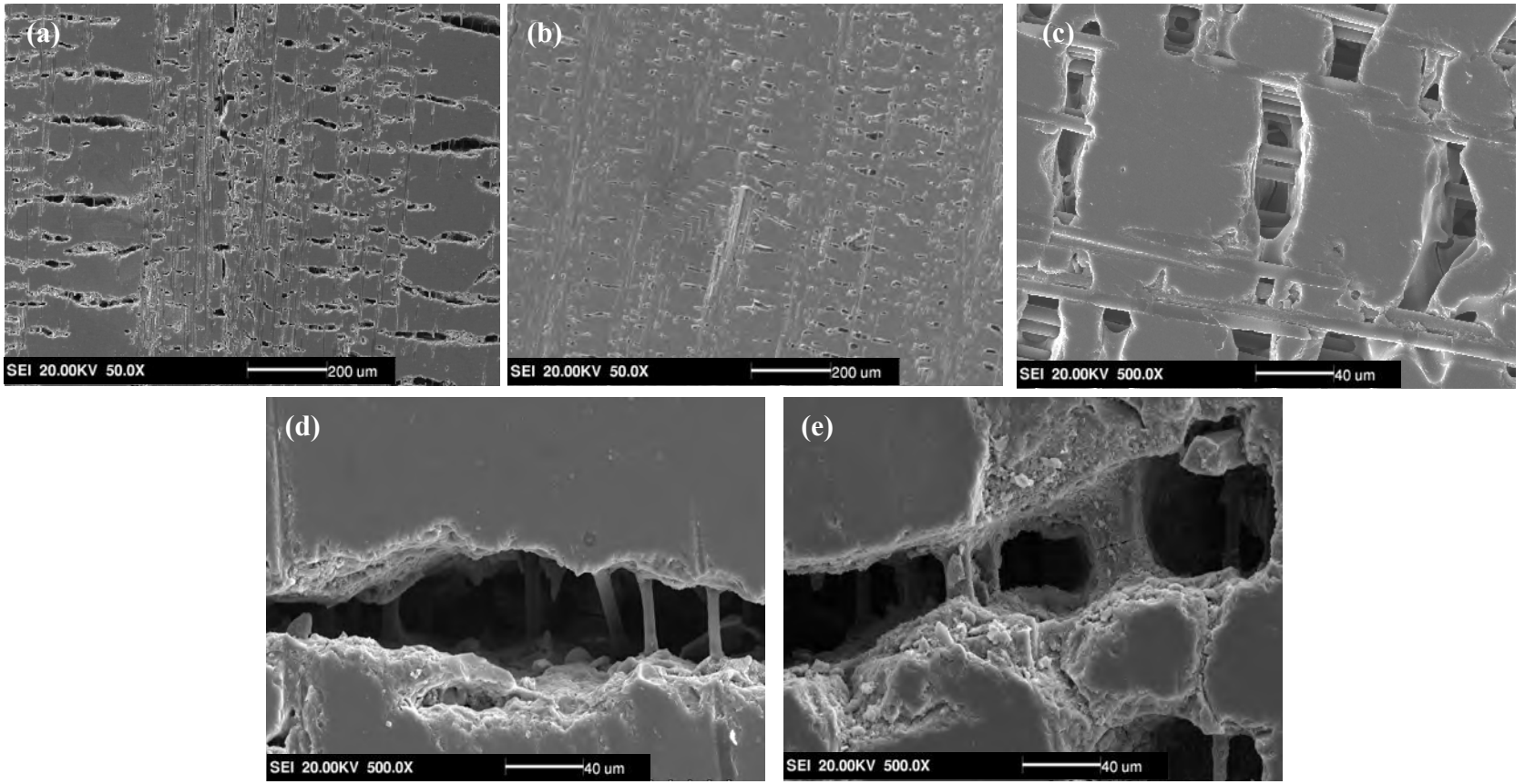

Fig. 3-7 Microstructure of polished cross section of:
(a) KC-1000, (b) KC-1100 (low magnification), (c) KC-1100 (high magnification), (d) KC-1300, (e) KC-1400

---- Peigang He, Dechang Jia. *Ceramics International*. 2010, 36 (4), 1447-1453.

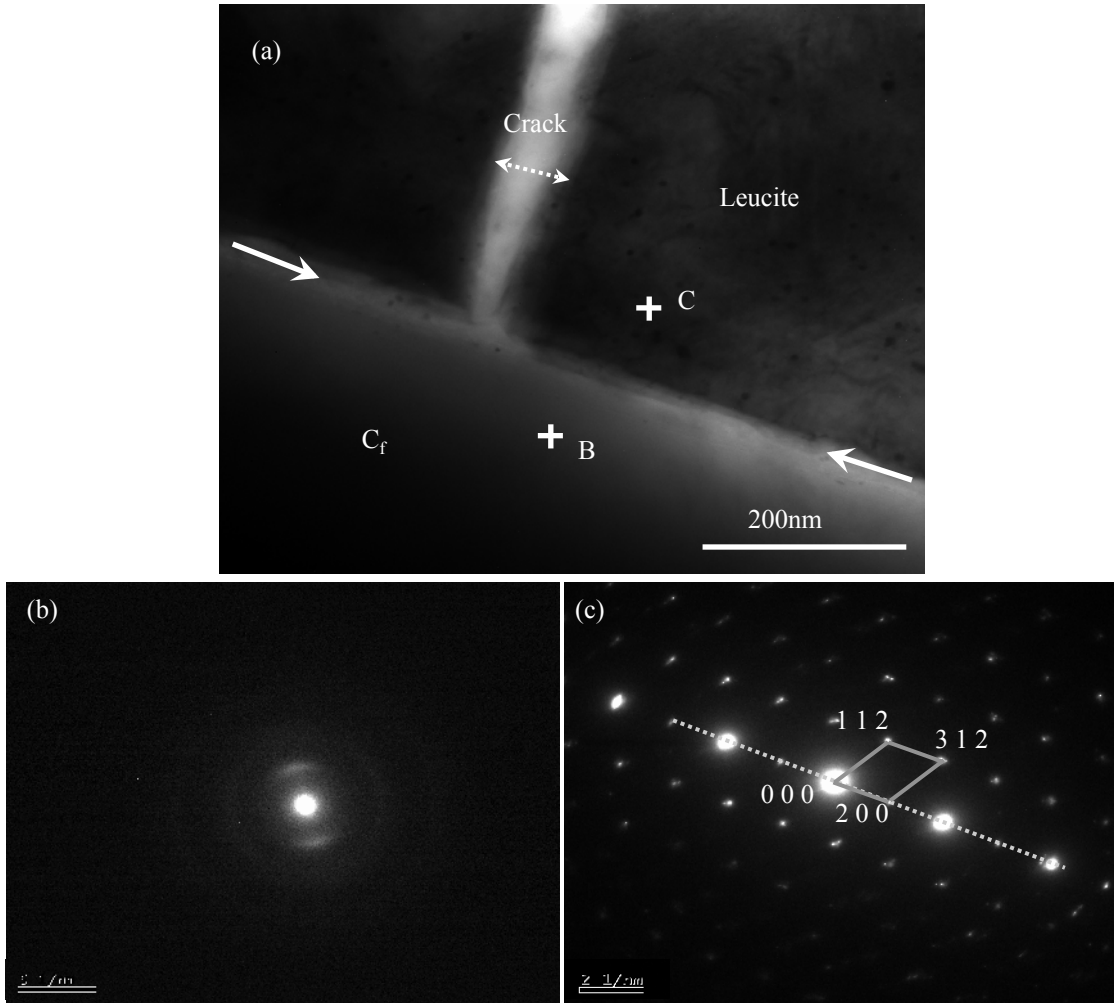

Fig. 3-8 Interface morphology of KC-1100:
(a) TEM image, (b) and (c) SAD paterns of carbon fiber and matrix in area of B and C

Residual stress: $$\sigma = \frac{(\alpha_m - \alpha_f) \times \Delta T E_f V_f}{V_f \times (\frac{E_f}{E_m} - 1) + 1} \qquad (3\text{-}2)$$

Table 3-1 Thermal residual stress in the composites during cooling process

ΔT (℃)	1100	1200	1300	1400
σ_a (MPa)	557.5	608.2	658.9	709.6
σ_r (MPa)	195.5	213.3	231.0	248.8

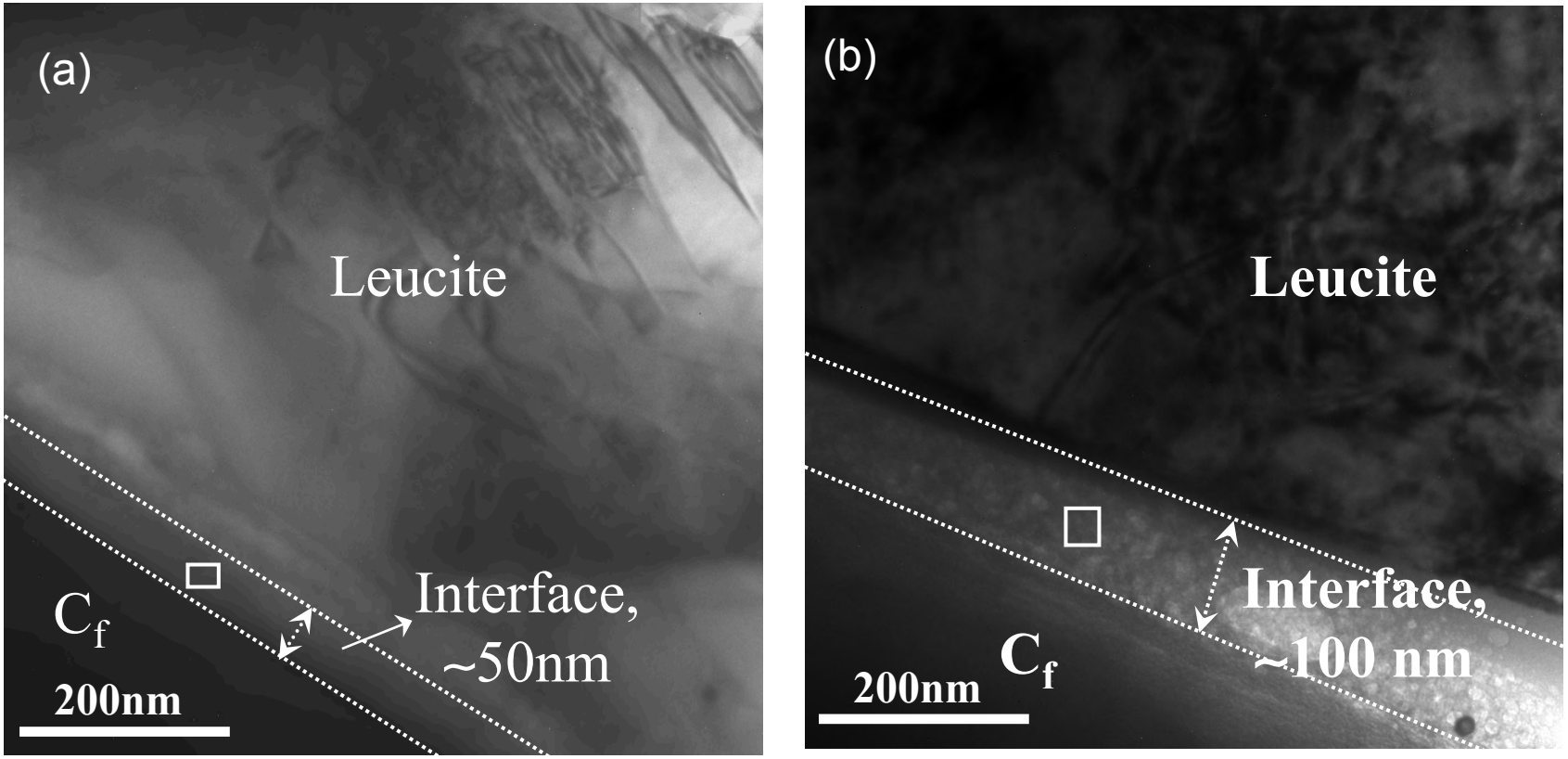

Fig. 3-9 Interface morphology of KC-1200 (a) and KC-1300°C(b)

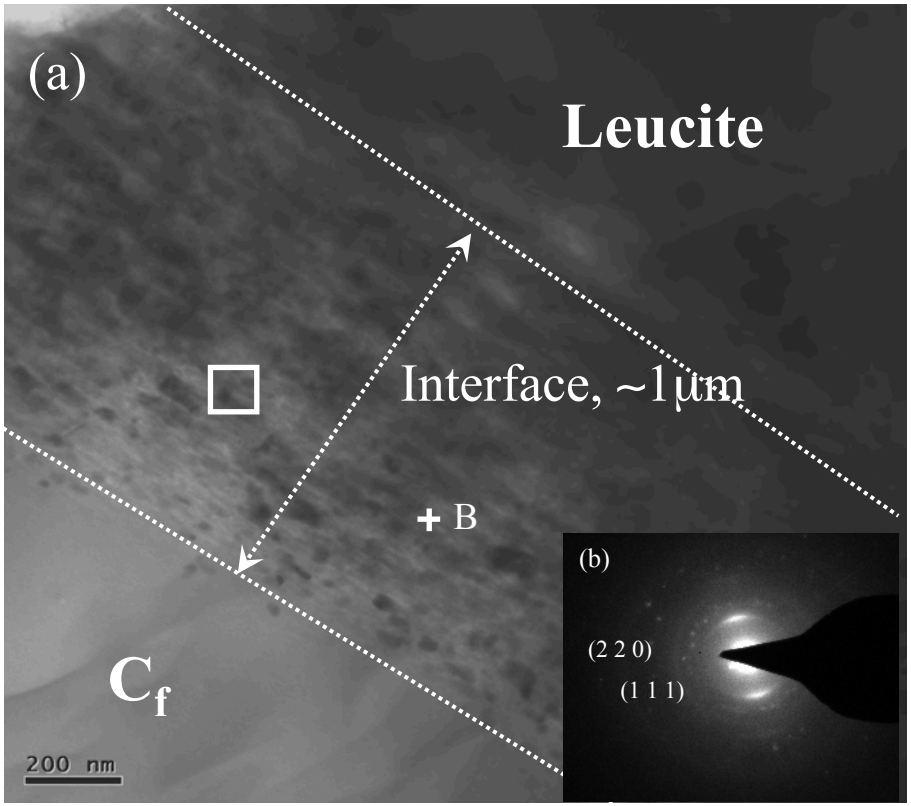

Fig. 3-10 Interface morphology of KC-1400

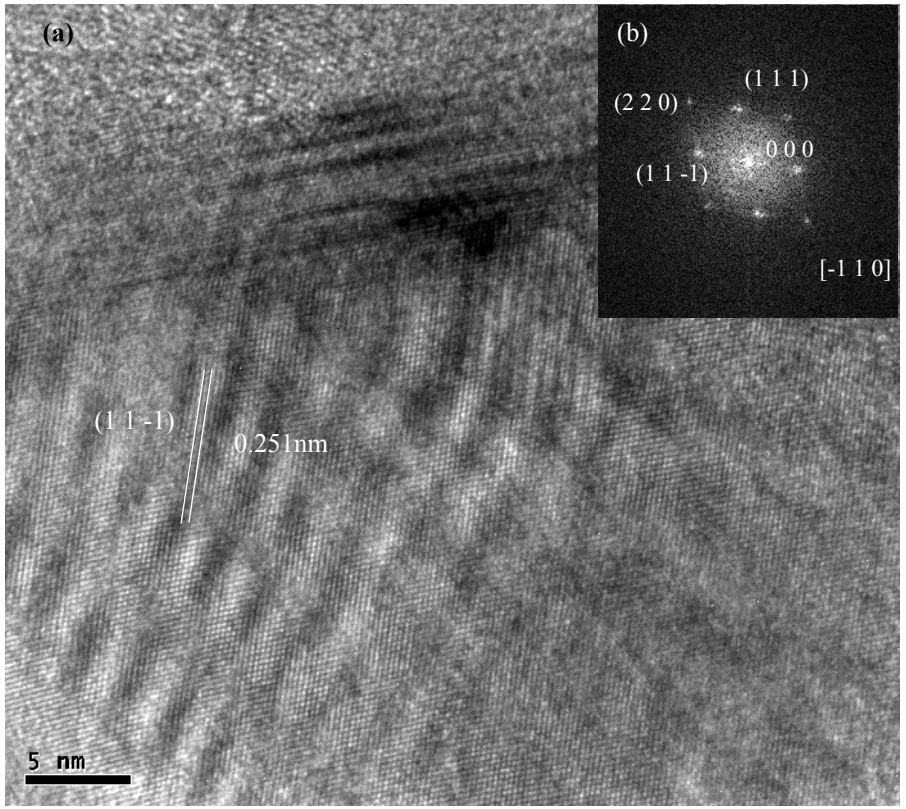

Fig. 3-11 HRTEM micrographs of area B in Fig.3-10: (a) HRTEM image and (b) FFT transformed image

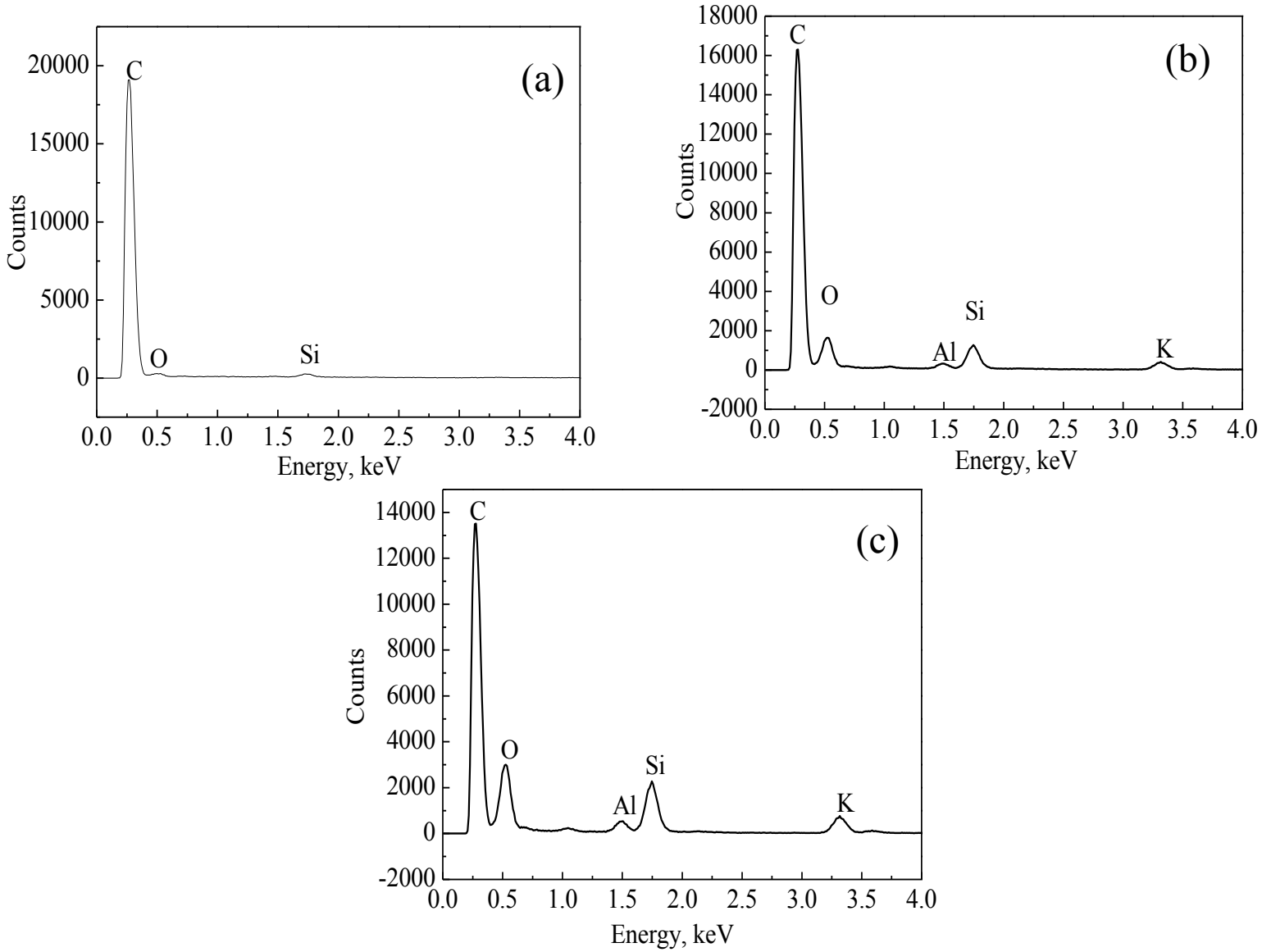

Fig. 3-12 Element distributions in the interface region:
(a) KC-1200, (b) KC-1300, (c) KC-1400

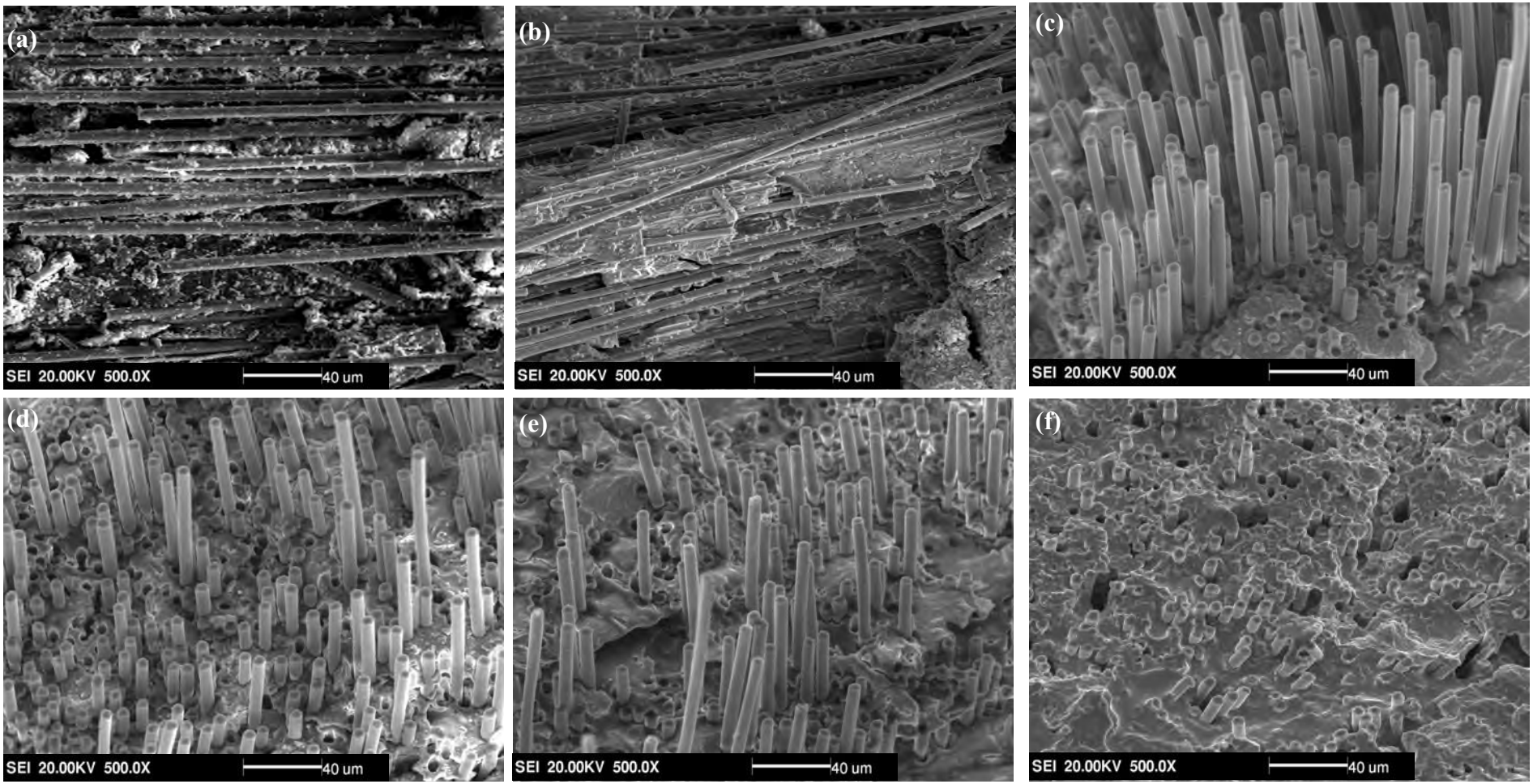

Fig. 3-13 Fractographs of C_f/KGP composites heat treated at different temperature: (a) KC-B, (b) KC-1000, (c) KC-1100, (d) KC-1200, (e) KC-1300, (f) KC-1400

---- Peigang He, Dechang Jia. *Ceramics International*. 2010, 36 (4), 1447-1453.

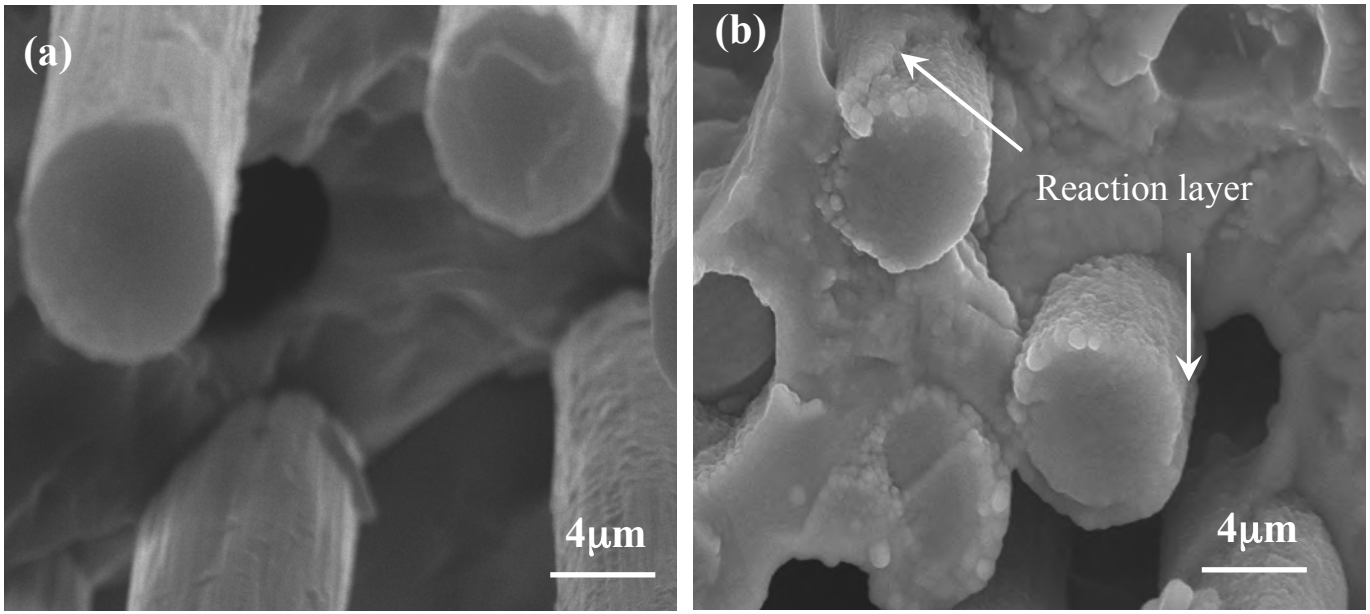

Fig. 3-14 Magnified fractograph of (a) KC-1100, (b) KC-1400

---- Peigang He, Dechang Jia. *Ceramics International*. 2010, 36 (4), 1447-1453.

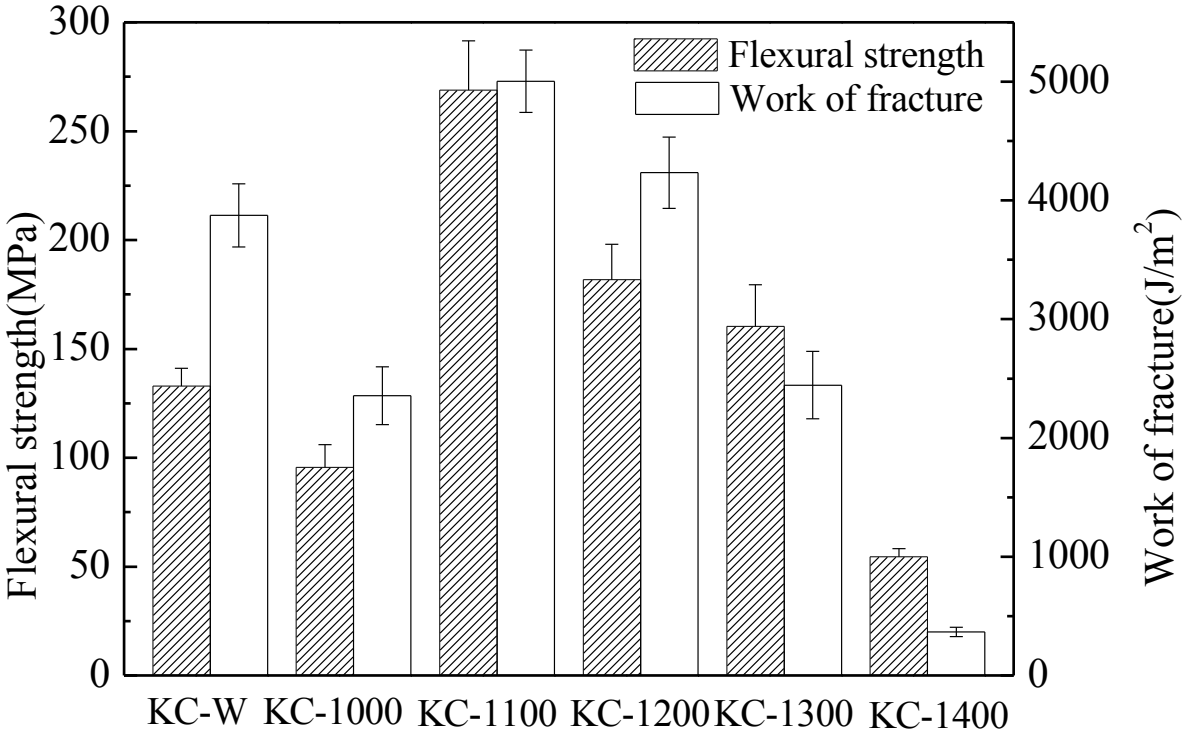

Fig. 3-15 Variations of flexural strength and work of fracture of C_f/KGP composites heat treated at different temperatures

---- Peigang He, Dechang Jia. *Ceramics International*. 2010, 36 (4), 1447-1453.

Table 3-2 Mechanical properties of geopolymer and C_f/KGP composites after heat treatment

Samples	Flexural strength (MPa)	Work of fracture ($J \cdot m^{-2}$)	Fracture toughess ($MPa \cdot m^{1/2}$)	Elastic modulus (GPa)
Geopolymer	12.3±1.2	—	0.2±0.04	10.3±1.2
Leucite ceramic	70.0±6.8	—	1.3±0.16	65.0±6.3
KC-W	132.9±8.2	3874.5±266.8	—	36.5±3.4
KC-1000	95.6±10.5	2354.8±243.6	—	30.4±4.1
KC-1100	268.9 ±14.6	5003.4±254.4	7.21±0.87	67.4±4.2
KC-1200	181.7±16.3	4233.4±299.5	6.57±0.64	55.9±4.8
KC-1300	160.3±19.2	2444.6±283.2	4.9±0.57	50.6±3.6
KC-1400	54.6±3.7	366.6±37.5	1.05±0.31	41.5±4.2

---- Peigang He, Dechang Jia. *Ceramics International*. 2010, 36 (4), 1447-1453.

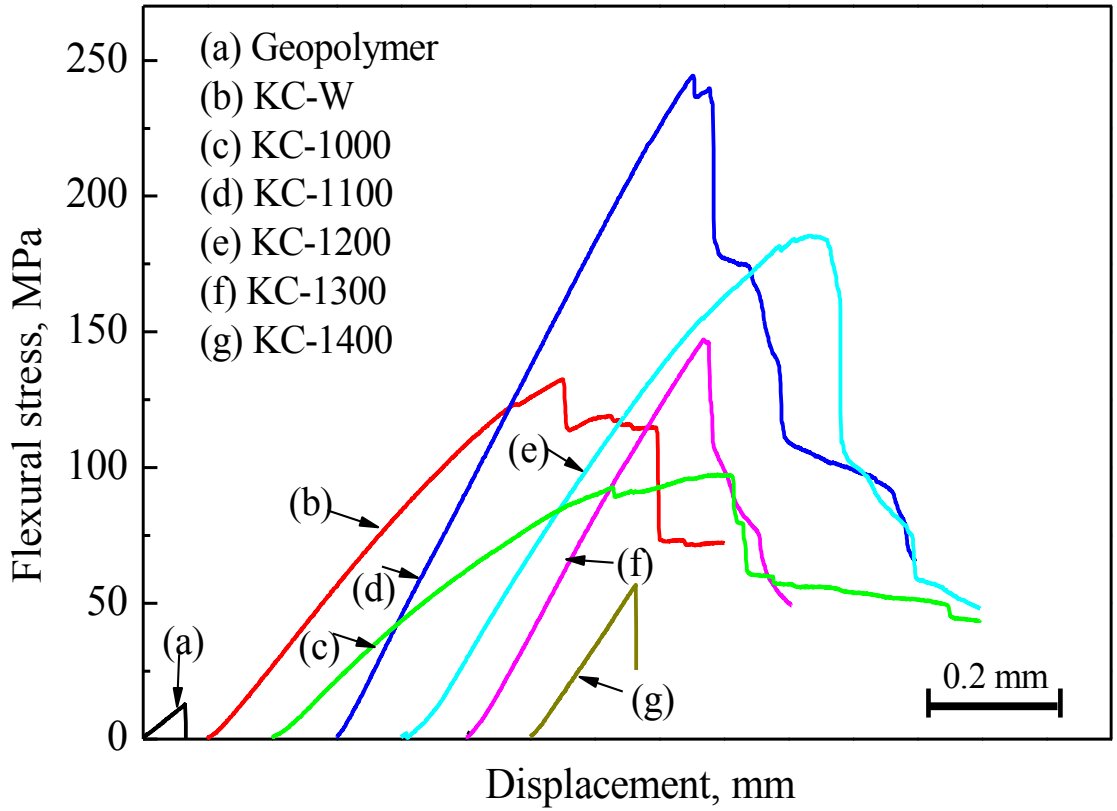

Fig. 3-16 Flexural stress-displacement curves of geopolymer and C_f/KGP composites heat treated at different temperatures

---- Peigang He, Dechang Jia. *Ceramics International*. 2010, 36 (4), 1447-1453.

3.2 Effects of heat treatment on the properties of C_f/CsKGP

- **Carbon fiber**: Unidirectional
- **Matrix**: $0.8K_2O \cdot 0.2Cs_2O \cdot Al_2O_3 \cdot 5SiO_2 \cdot 11H_2O$
- **Composites without and after heat treatment were denoted as:**

  CsKC-W, CsKC-1000, CsKC-1100, CsKC-1150, CsKC-1200 and CsKC-1300, respectively
- **Fiber contents**: 20vol% for CsKC-W and ~25vol% for others

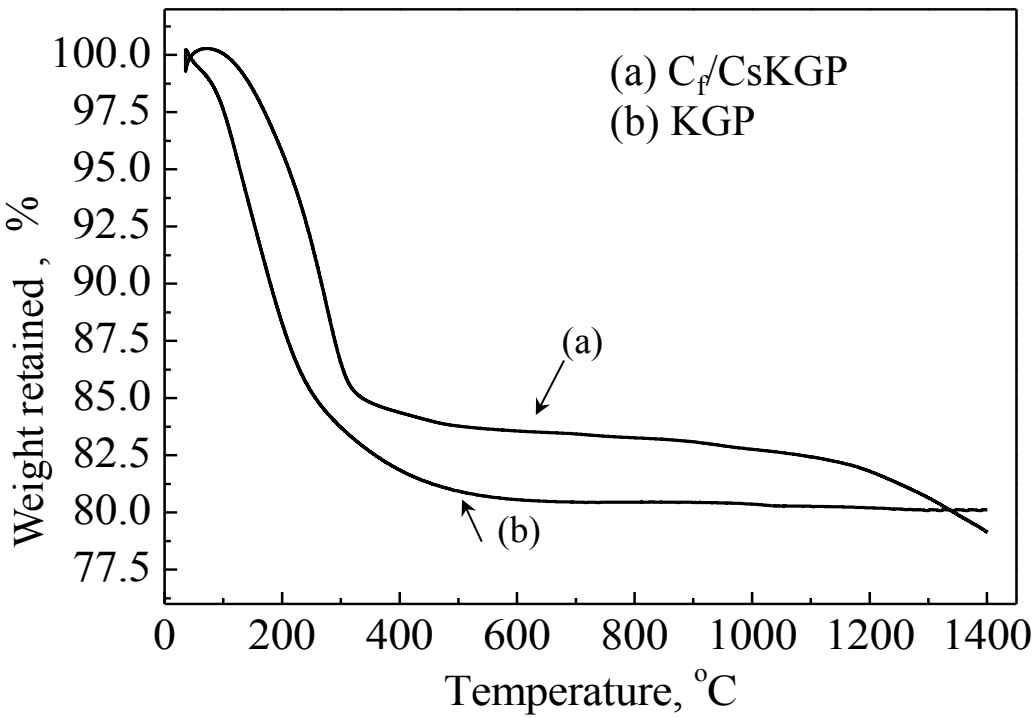

Fig. 3-17 Weight retained of KGP and C_f/CsKGP composites

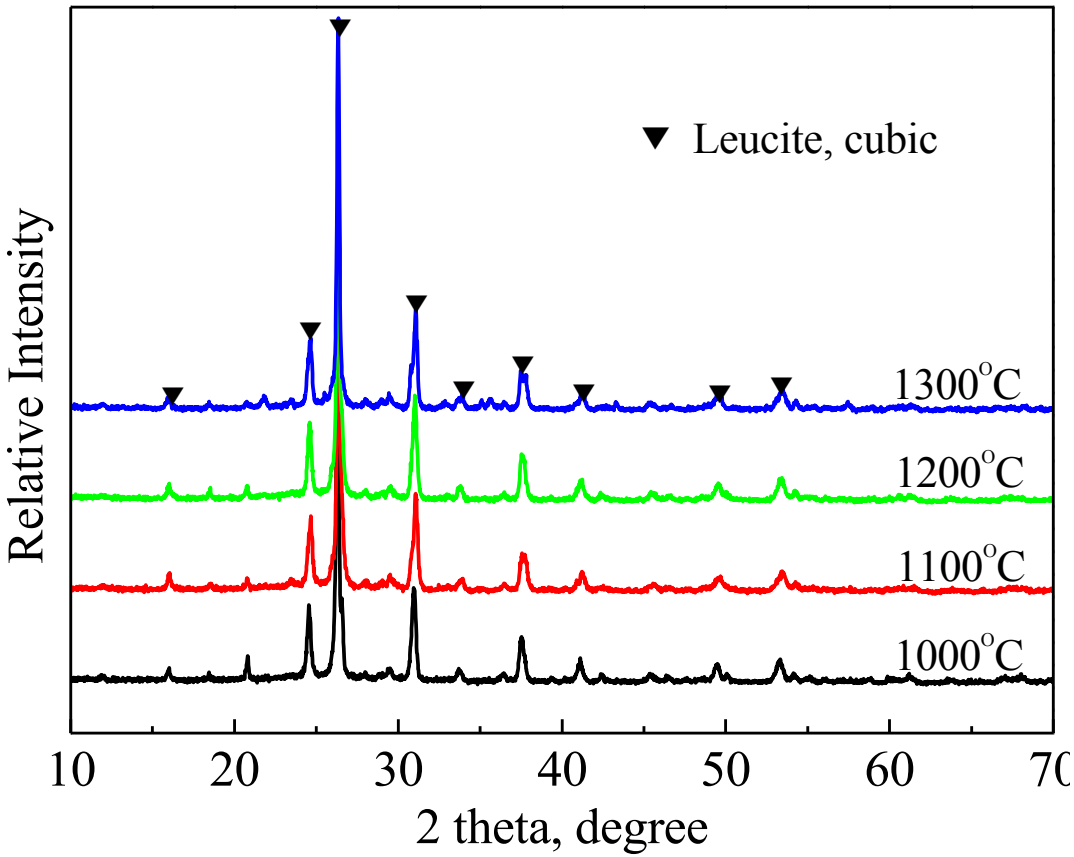

Fig. 3-18 XRD patterns of C_f/CsKGP heat treated at different temperatures

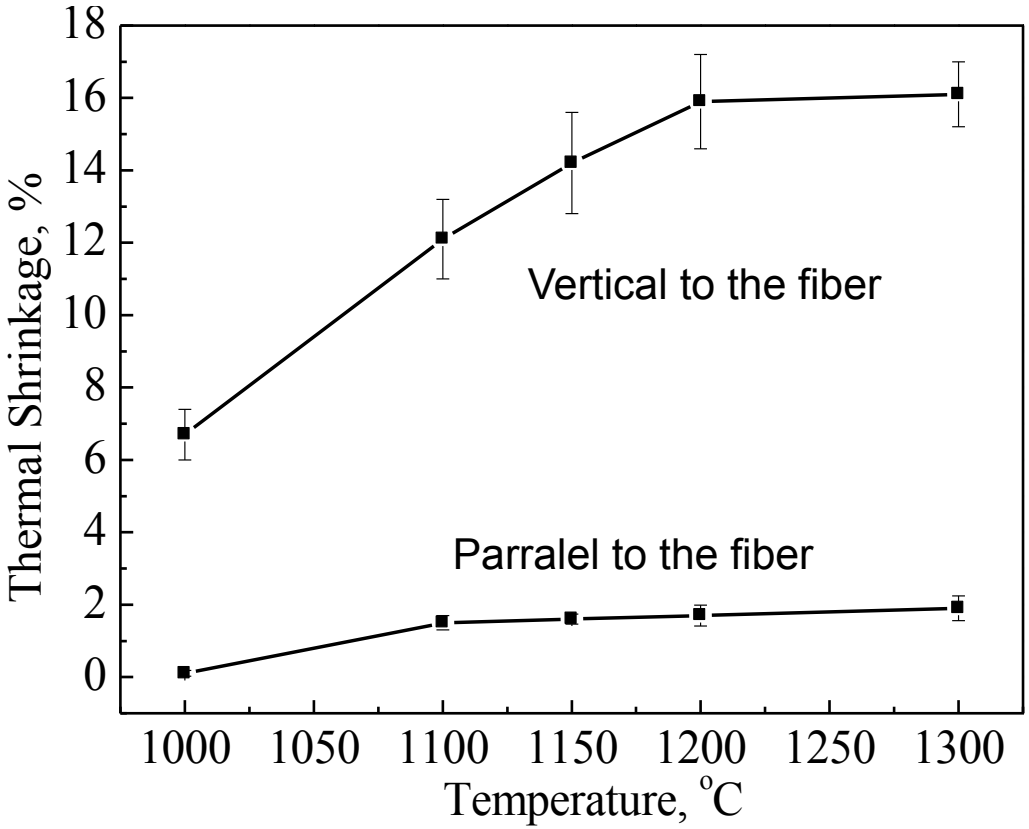

Fig. 3-19 Thermal shrinkages of C_f/CsKGP heat treated at different directions

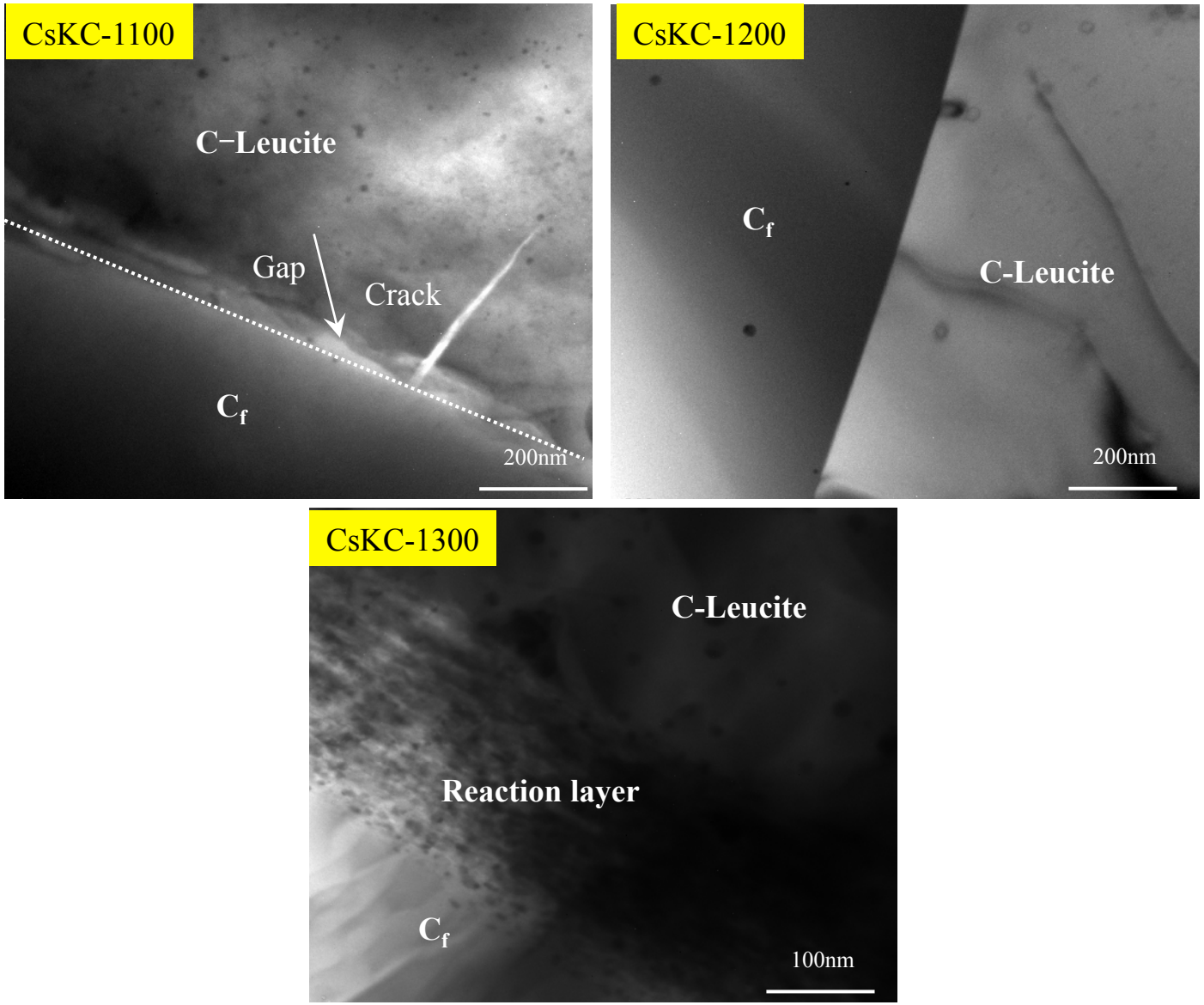

Fig. 3-20 Interface morphology of C_f/CsKGP heat treated at different temperatures : (a) CsKC-1100, (b) CsKC-1200, (c) CsKC-1300

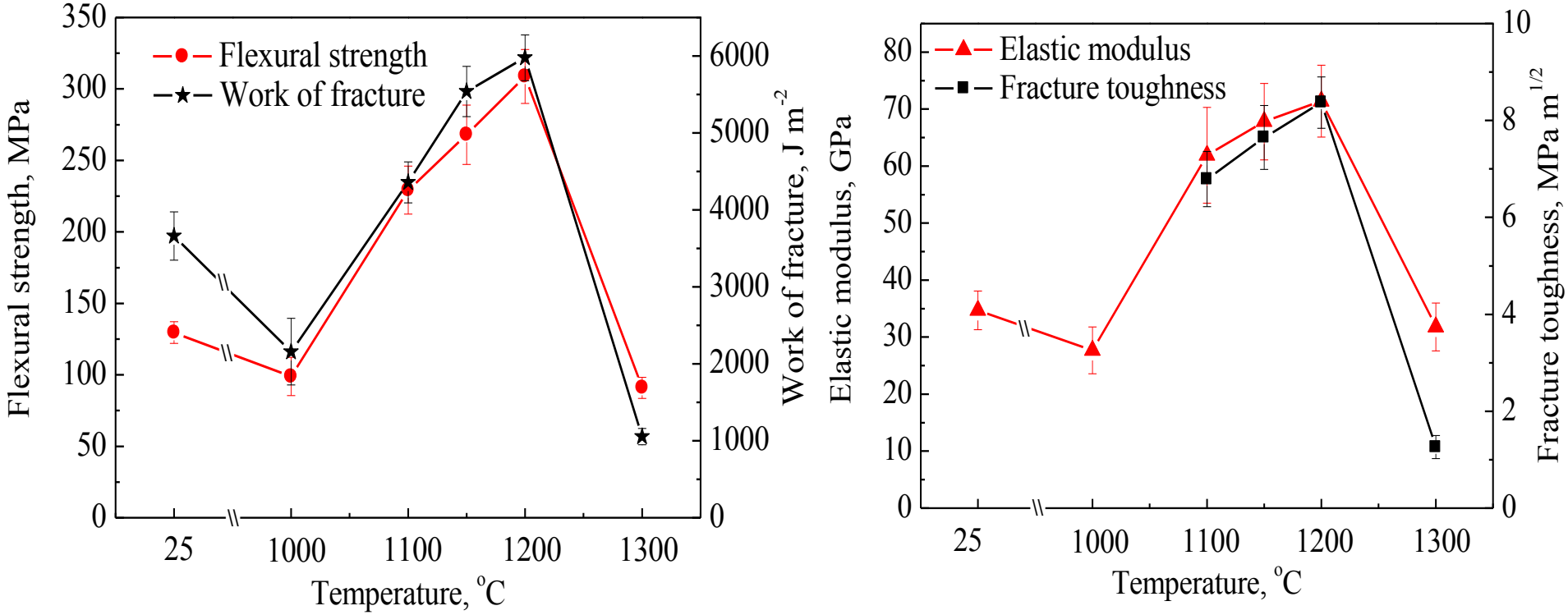

Fig. 3-21 Variations of the mechanical properties of C_f/CsKGP heat treated at different temperatures: (a) Flexural strength and work of fracture, (b) Young's modulus and fracture toughness

Table 3-3 Mechanical properties of C_f/CsKGP composites heat treated at different temperature

Samples	Flexural strength (MPa)	Work of fracture ($J \cdot m^{-2}$)	Fracture toughess (MPa $m^{1/2}$)	Elastic modulus (GPa)
CsKC-W	129.6±7.5	3659.9±314.7	—	34.7±3.4
CsKC-1000	98.8±13.4	2158.7±431.5	—	27.7±4.1
CsKC-1100	229.2±16.8	4357.9±267.7	6.79±0.57	61.9±8.4
CsKC-1150	268.0±20.7	5538.4±327.5	7.65±0.66	67.8±6.7
CsKC-1200	278.7±18.9	5977.4±297.1	8.37±0.53	71.4±6.3
CsKC-1300	90.9±7.4	1054.8±106.7	1.26±0.24	31.8±4.2

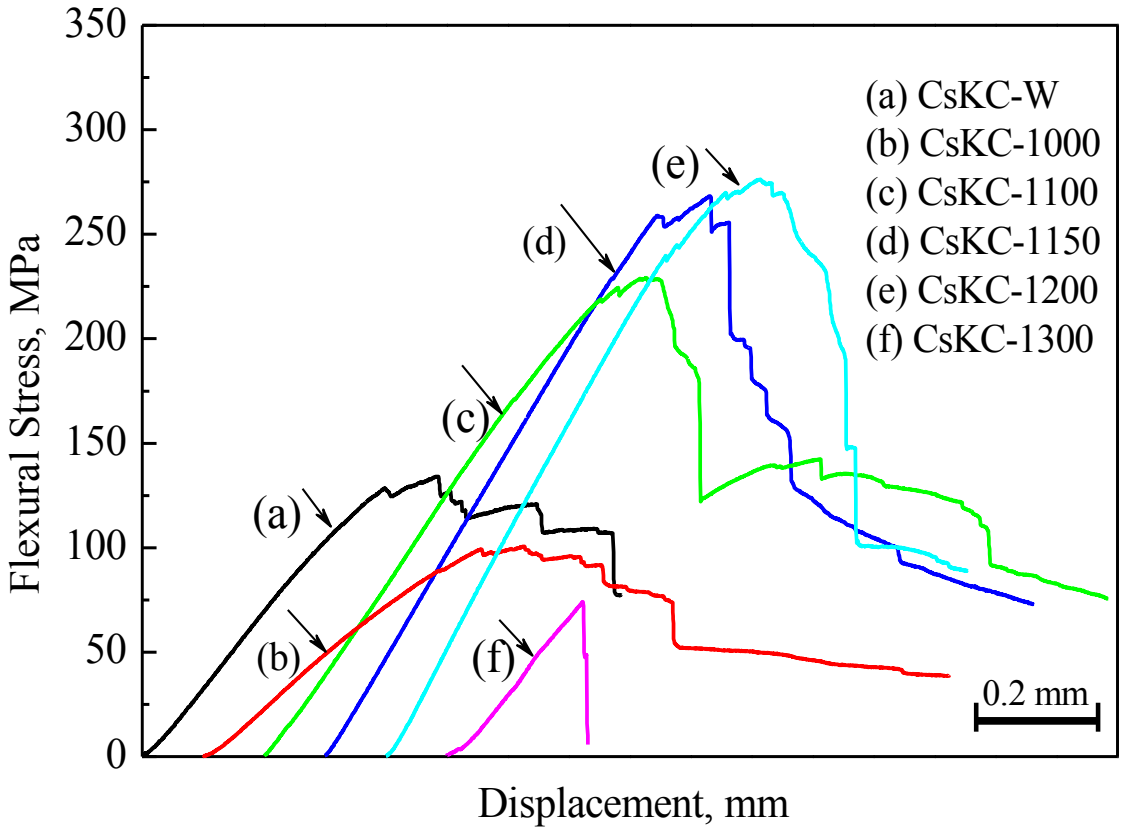

Fig. 3-22 Flexural stress–displacement curves of C_f/CsKGP heat treated at different temperatures

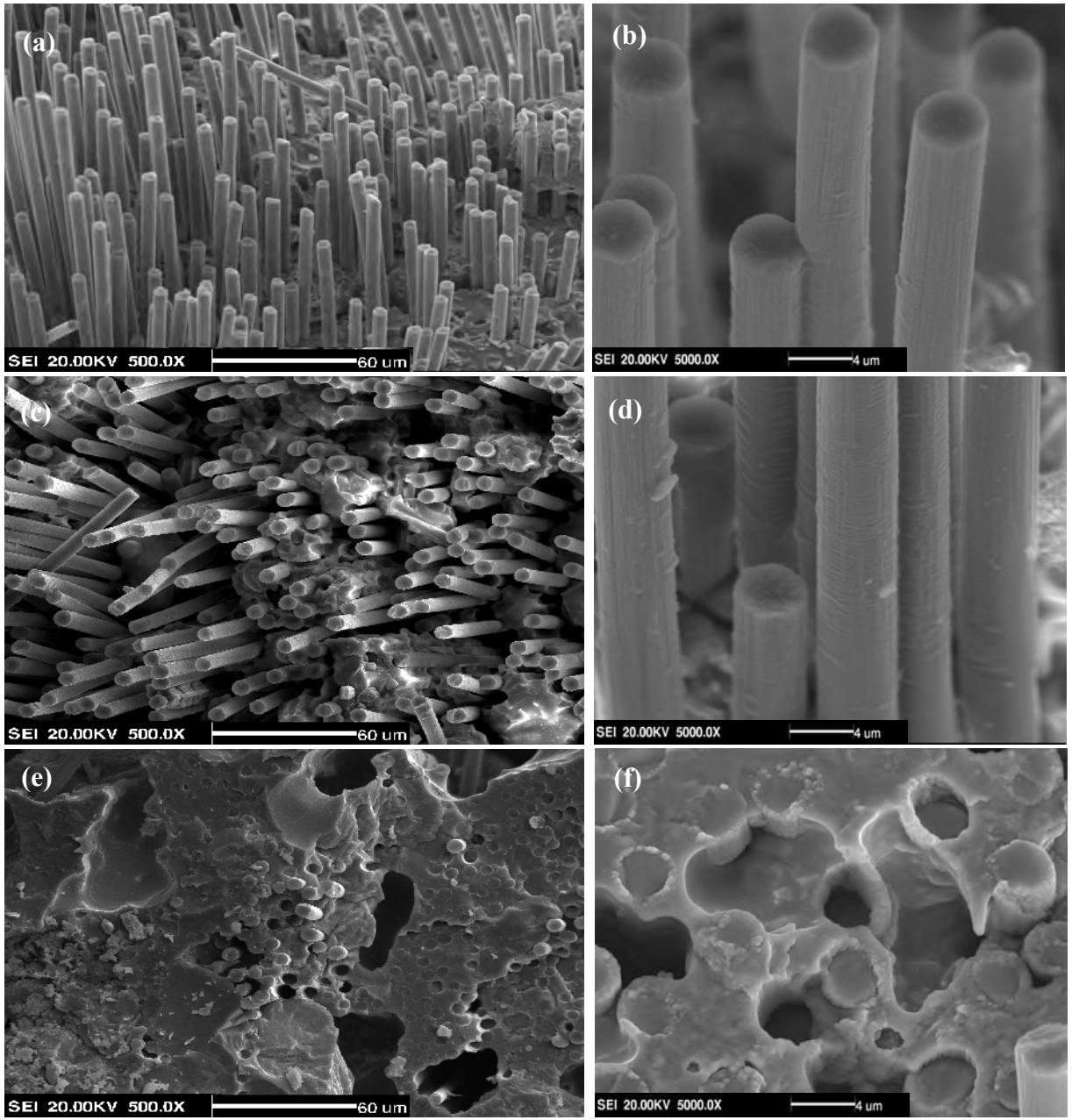

Fig. 3-23 Fractographs of C_f/CsKGP composites heat treated at different temperature: (a), (b) 1100°C, (c), (d) 1200°C and (e), (f) 1300°C

3.3 Summary

- After proper heat treatment, the C_f/geopolymer composite can be directly converted into the carbon fiber reinforced leucite ceramic matrix composites, and mechanical properties could be greatly enhanced.
- The property improvement can be attributed to the densified and crystallized matrix, and the enhanced fiber/matrix interface bonding based on the fine-integrity of carbon fibers.
- For the composite heat treated at higher temperature($\geq 1300^{o}$ C), the mechanical properties lowered substantially and it tended to fracture in a very brittle manner owing to the seriously degraded carbon fibers.

4. Sol-SiO_2 impregnation on the ambient and high temperature mechanical properties of C_f/leucite composites

4.1 Microstructure of the composites after repeated impregnation

4.2 Room temperature mechanical properties

4.3 Non-isothermal oxidation of the composites

4.4 High-temperature mechanical properties and fracture mechanism

4.5 Summary

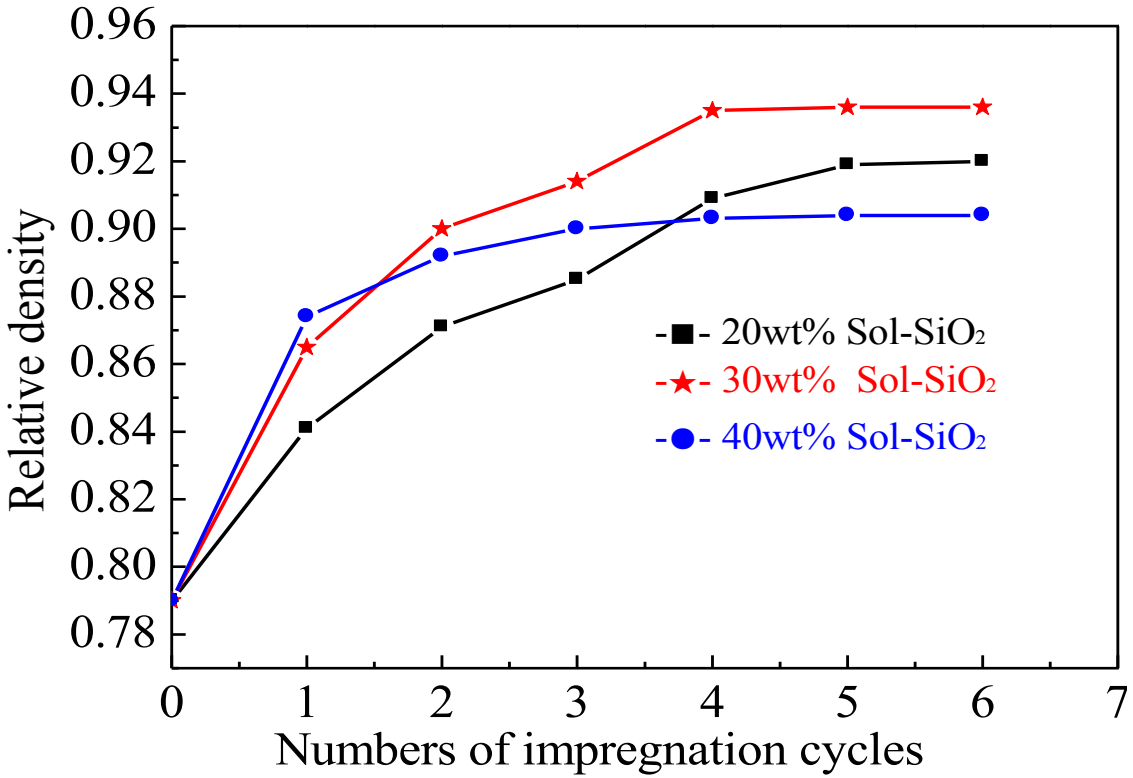

Fig. 4-1 Relative density vs. number of impregnation/drying cycles with different sol-SiO_2 concentration

---- Peigang He, Dechang Jia. *Journal of the European Ceramic Society*. 2010, 30 (15), 3053–3061.

4.1 Microstructure of the composites after repeated impregnation

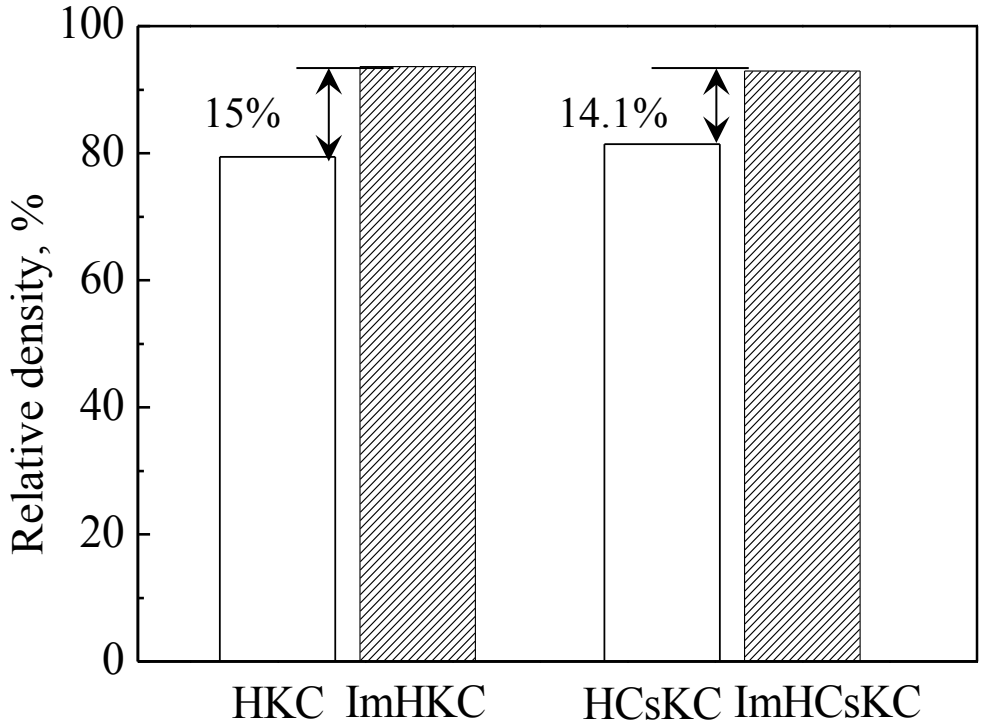

Fig. 4-2 Relative density of the composites before and after sol-SiO_2 impregnation

---- Peigang He, Dechang Jia. *Journal of the European Ceramic Society*. 2010, 30 (15), 3053–3061.

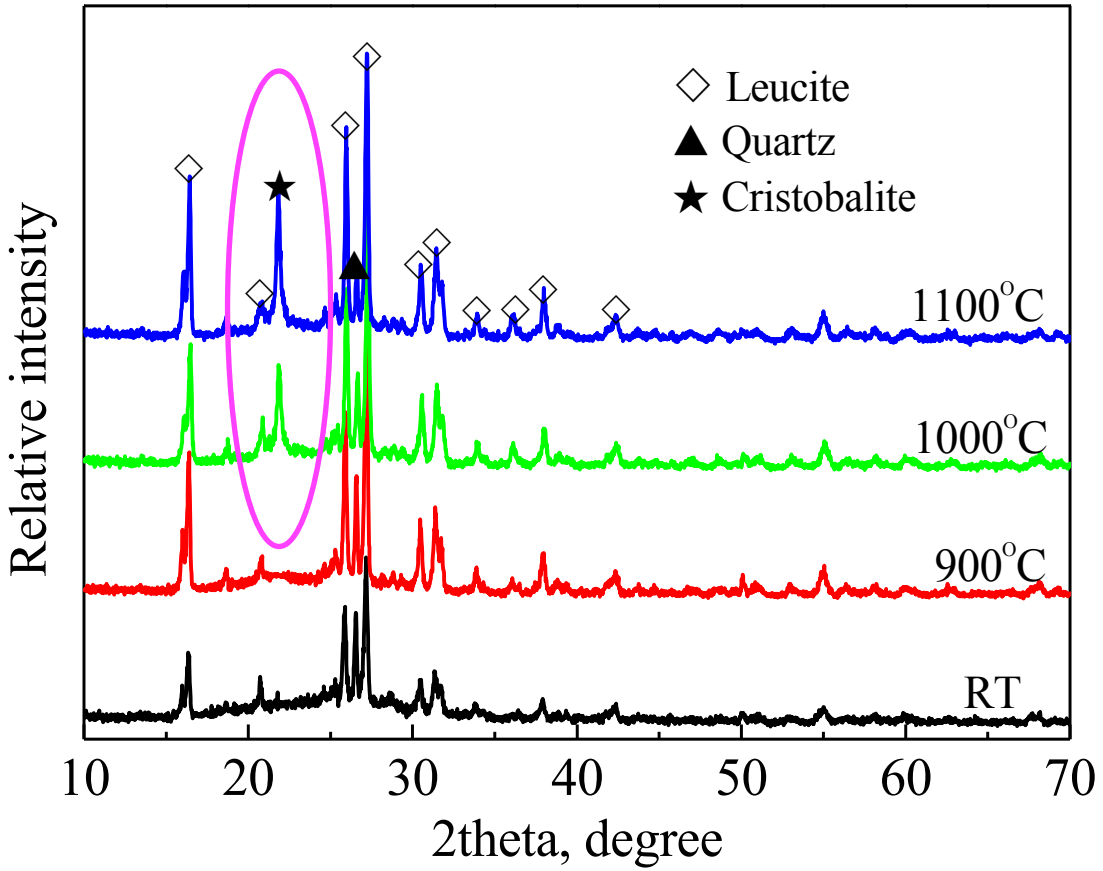

Fig. 4-3 XRD patterns of the impregnated composite treated at different temperatures

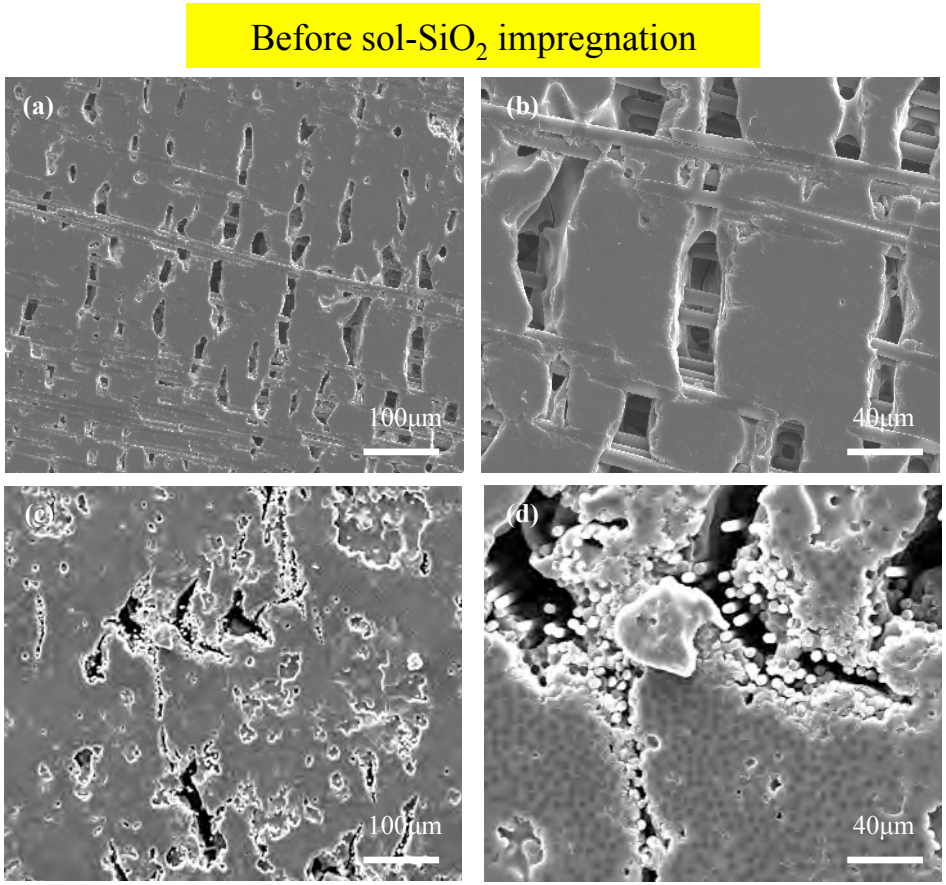

Fig. 4-4 Microstructures of the polished cross section of HKC composite:(a), (b) in the axial direction of fibers; (c), (d) in the radial direction

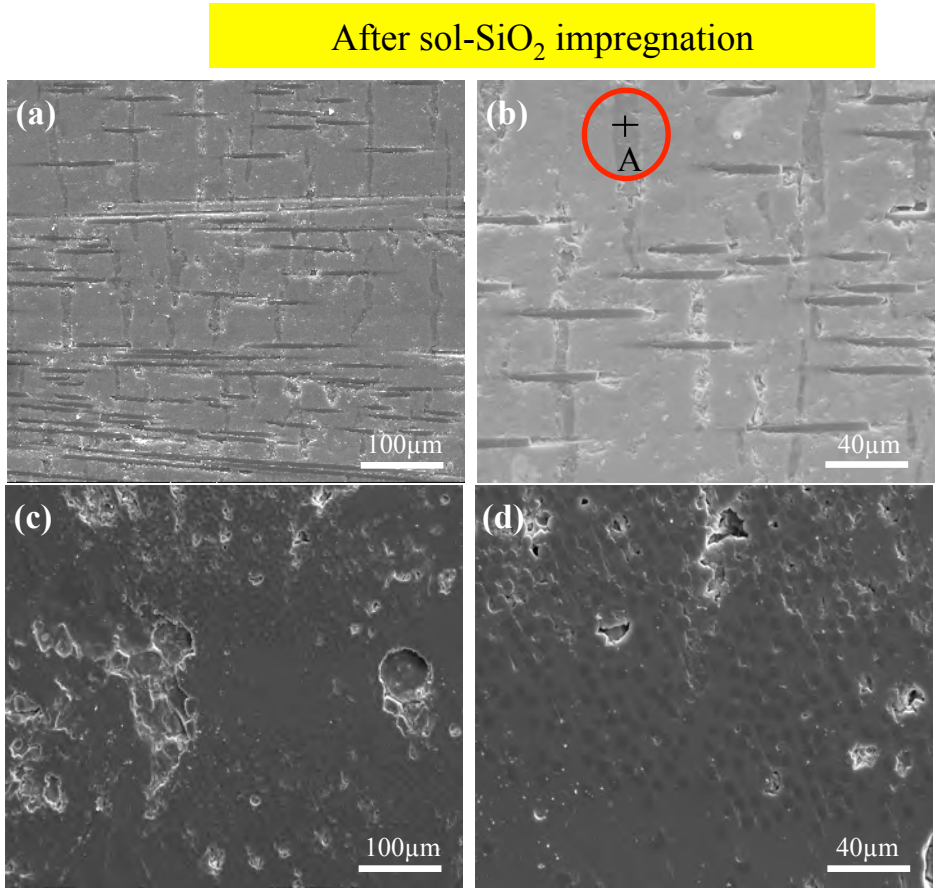

Fig. 4-5 Microstructure of the polished cross section of ImHKC composite: (a), (b) in the axial direction of fibers; (c),(d) in the radial direction

---- Peigang He, Dechang Jia. *Journal of the European Ceramic Society*. 2010, 30 (15), 3053–3061.

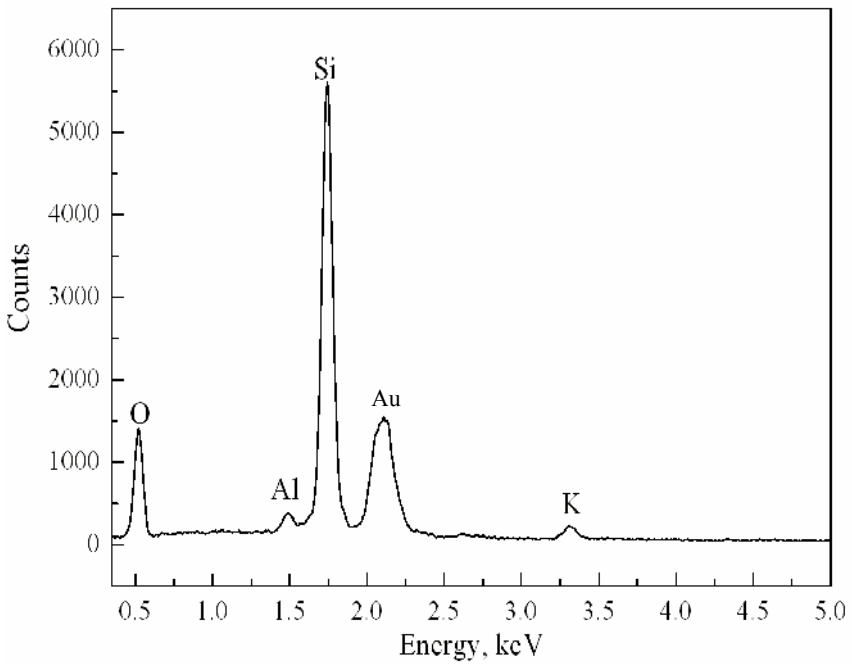

Fig. 4-6 Energy dispersive spectrum of point A in the Fig. 4-5

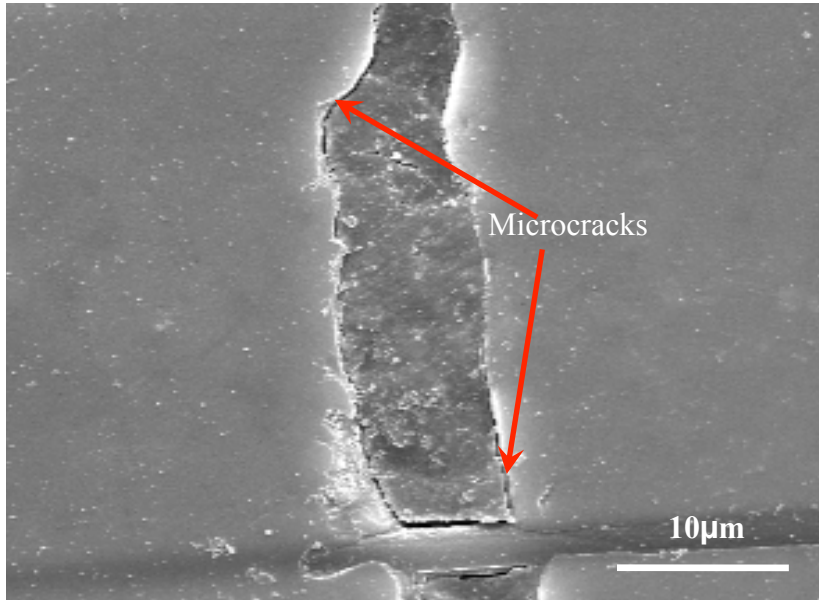

Fig. 4-7 Microstructure at a higher magnification of a sol-SiO_2 sealed crack

---- Peigang He, Dechang Jia. *Journal of the European Ceramic Society*. 2010, 30 (15), 3053–3061.

4.2 Room temperature mechanical properties

Flexural strength

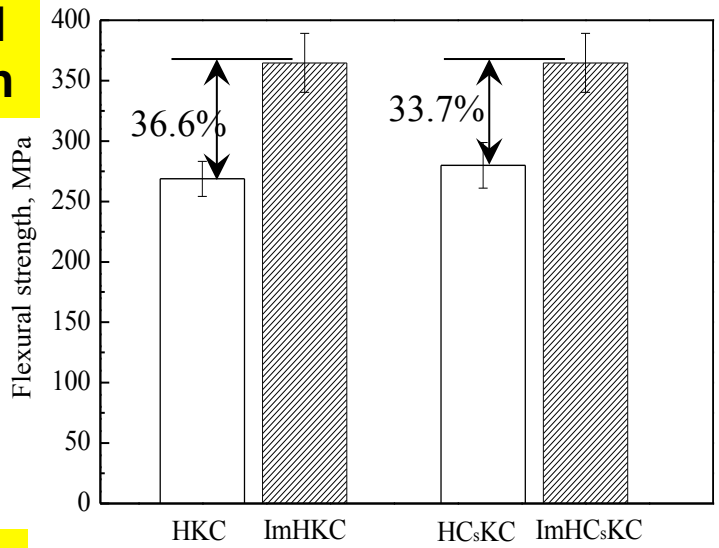

Young's Modulus

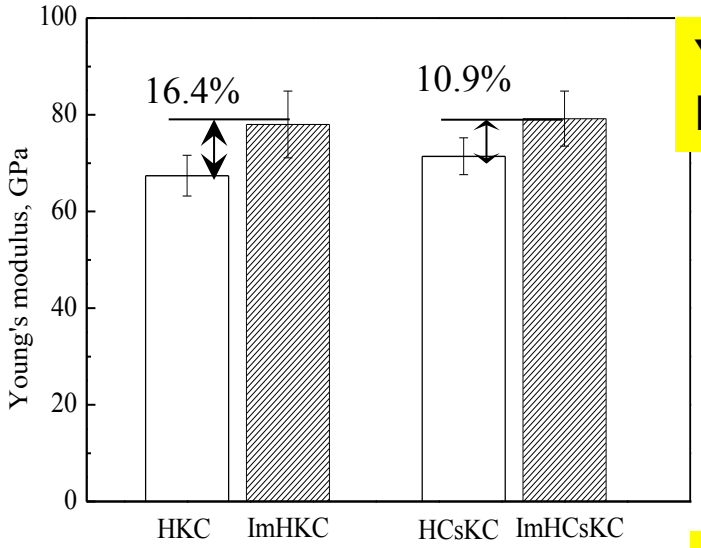

Fracture tougness

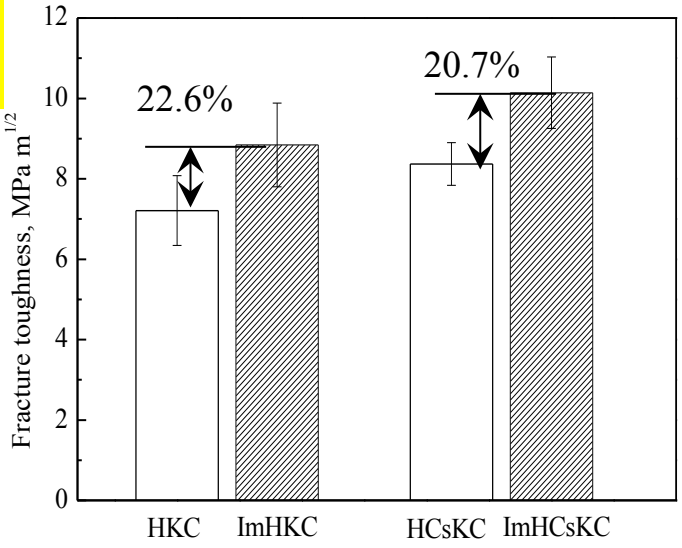

Work of fracture

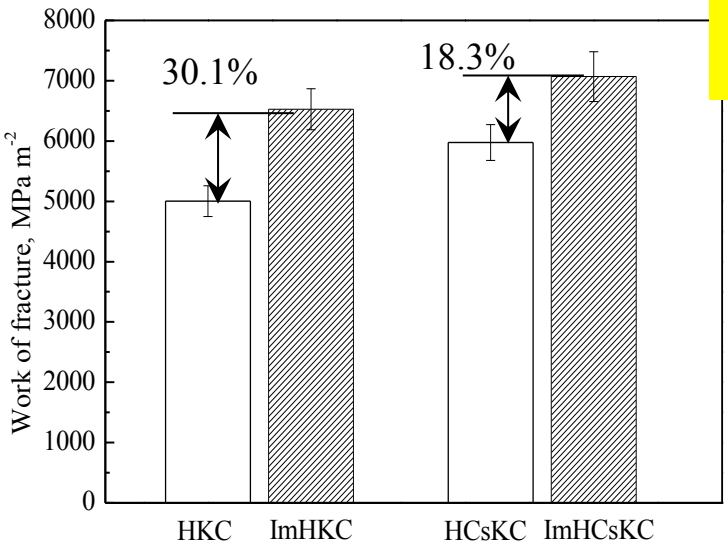

Fig.4-8 Mechanical properties of (Im)HKC and (Im)CsHKC

---- Peigang He, Dechang Jia. *Journal of the European Ceramic Society*. 2010, 30 (15), 3053–3061.

Table 4-1 Room temperature properties of HKC and ImHKC

Specimen	HKC	ImHKC
Density (g/cm^3)	1.81	2.16
Relative Density (%)	79.0	93.4
Flexural strength (MPa)	268.9 ±14.6	364.7±24.4
Young's modulus (GPa)	67.4±4.2	78.0±6.9
Fracture toughness ($MPa \cdot m^{1/2}$)	7.21±0.87	8.84±1.04
Work of fracture ($J \cdot m^{-2}$)	5003.4±254.4	6527.4±342.1

Table 4-2 Room temperature properties of HCsKC and ImHCsKC

Specimen	HCsKC	ImHCsKC
Density (g/cm^3)	1.85	2.28
Relative Density (%)	81.4	92.9
Flexural strength (MPa)	278.7±18.9	376.4±21.3
Young's modulus (GPa)	71.4±3.8	79.2±5.7
Fracture toughness ($MPa \cdot m^{1/2}$)	8.37±0.53	10.14±0.89
Work of fracture ($J \cdot m^{-2}$)	5977.4±297.4	7068.6±413.8

4.3 Non-isothermal oxidation behavior

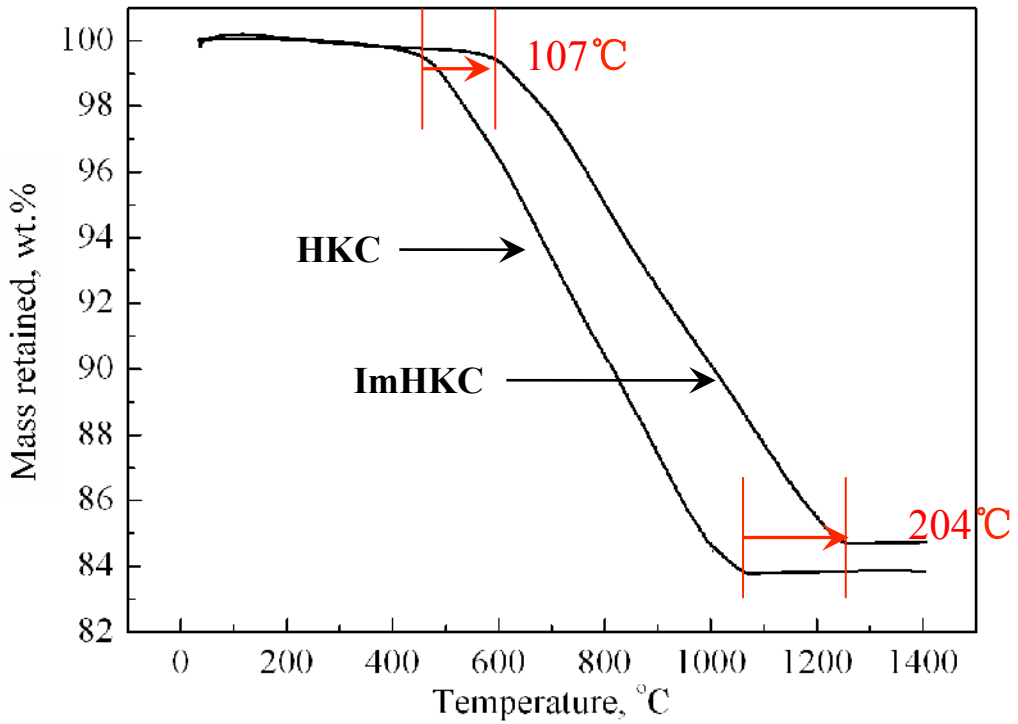

Fig. 4-9 Non-isothermal oxidation weight loss of the HKC and ImHKC composites

4.4 High-temperature mechanical properties

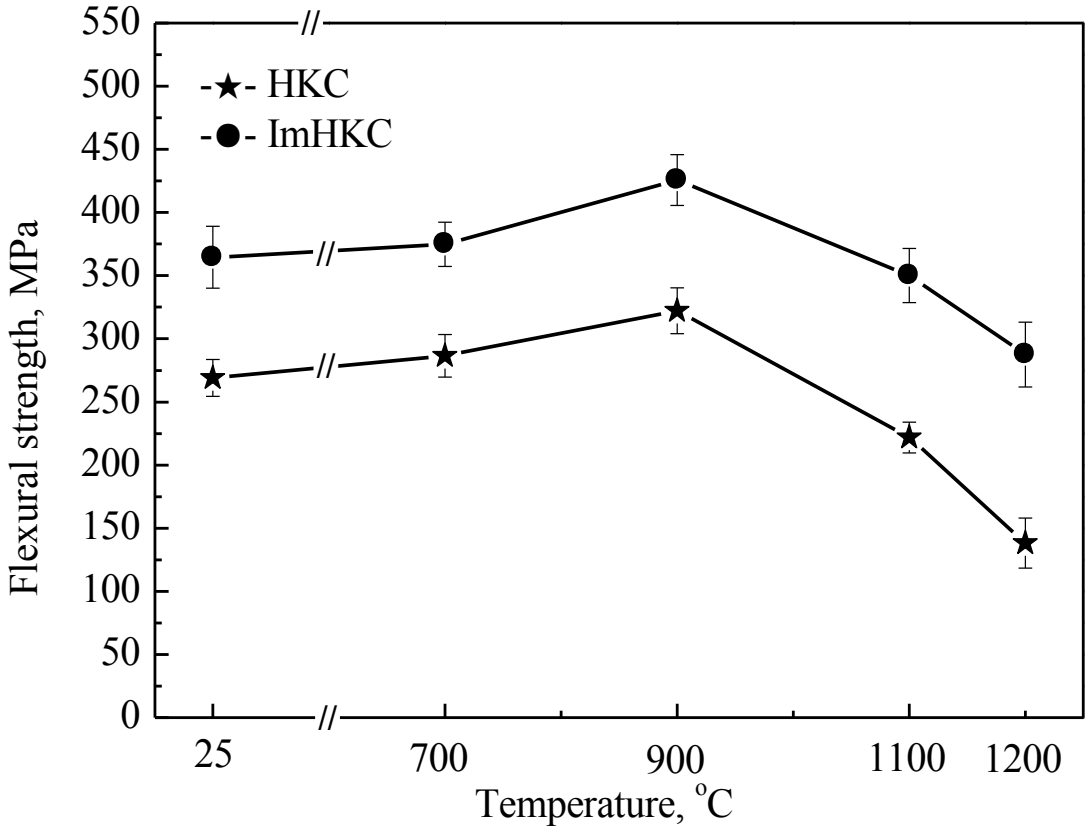

Fig. 4-10 Elevated temperature flexural strength of HKC and ImHKC

---- Peigang He, Dechang Jia. *Journal of the European Ceramic Society*. 2010, 30 (15), 3053–3061.

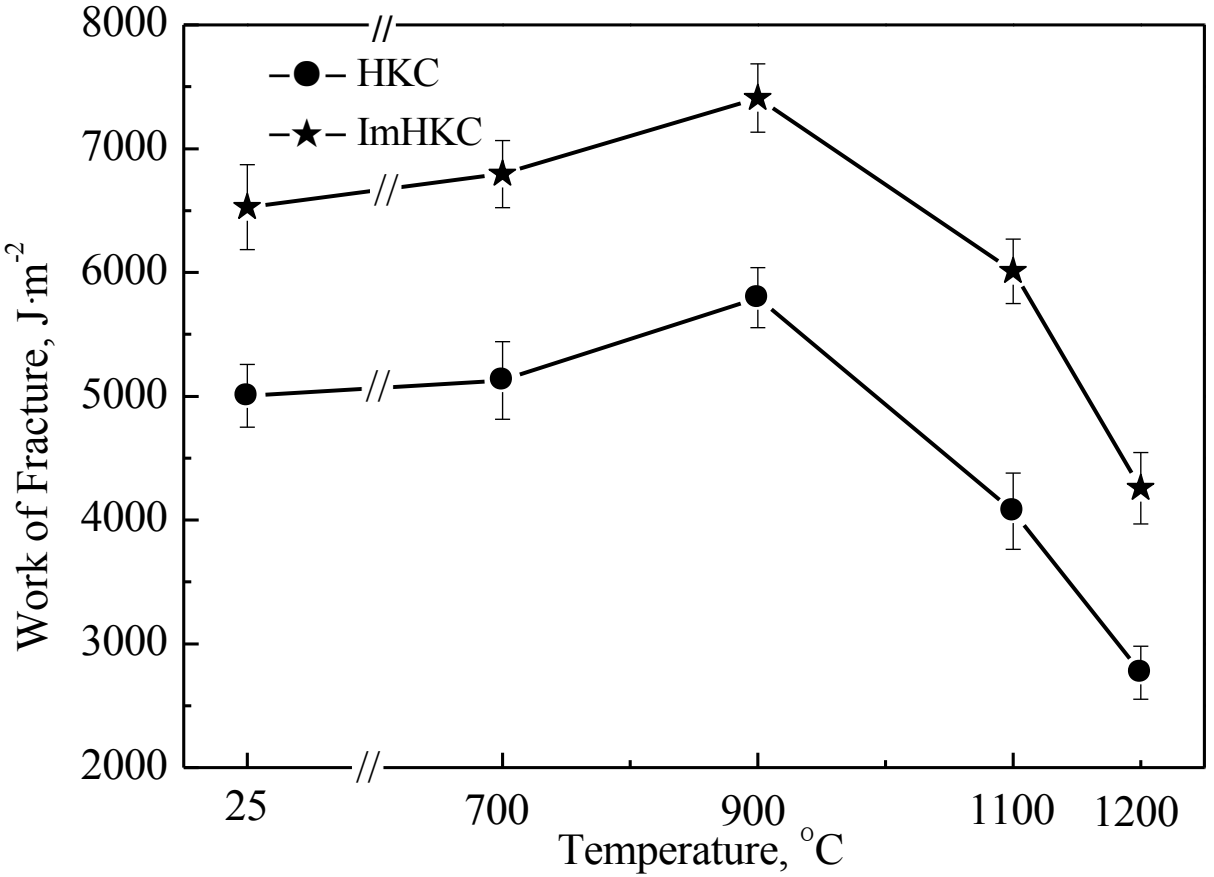

Fig. 4-11Elevated temperature work of fracture of HKC and ImHKC

---- Peigang He, Dechang Jia. *Journal of the European Ceramic Society*. 2010, 30 (15), 3053–3061.

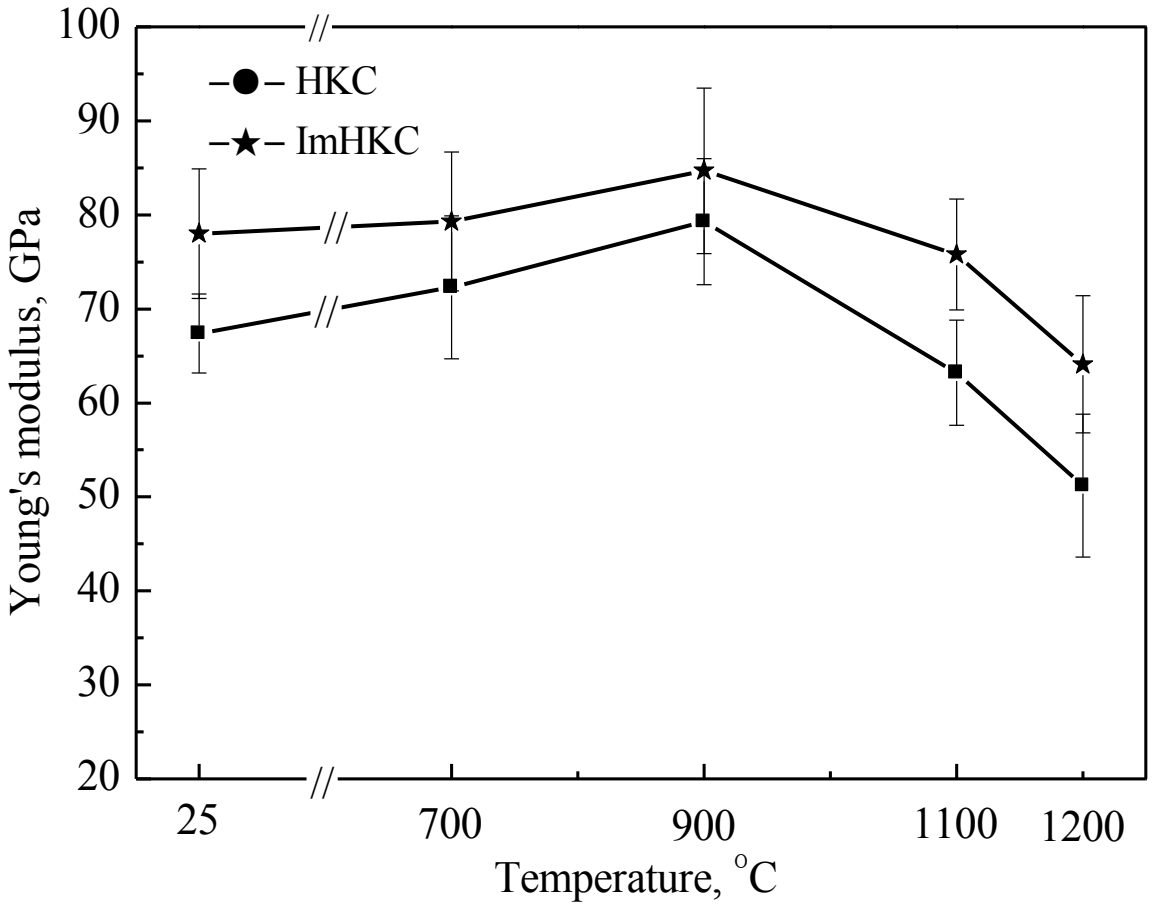

Fig. 4-12 Elevated temperature Young's modulus of HKC and ImHKC

---- Peigang He, Dechang Jia. *Journal of the European Ceramic Society*. 2010, 30 (15), 3053–3061.

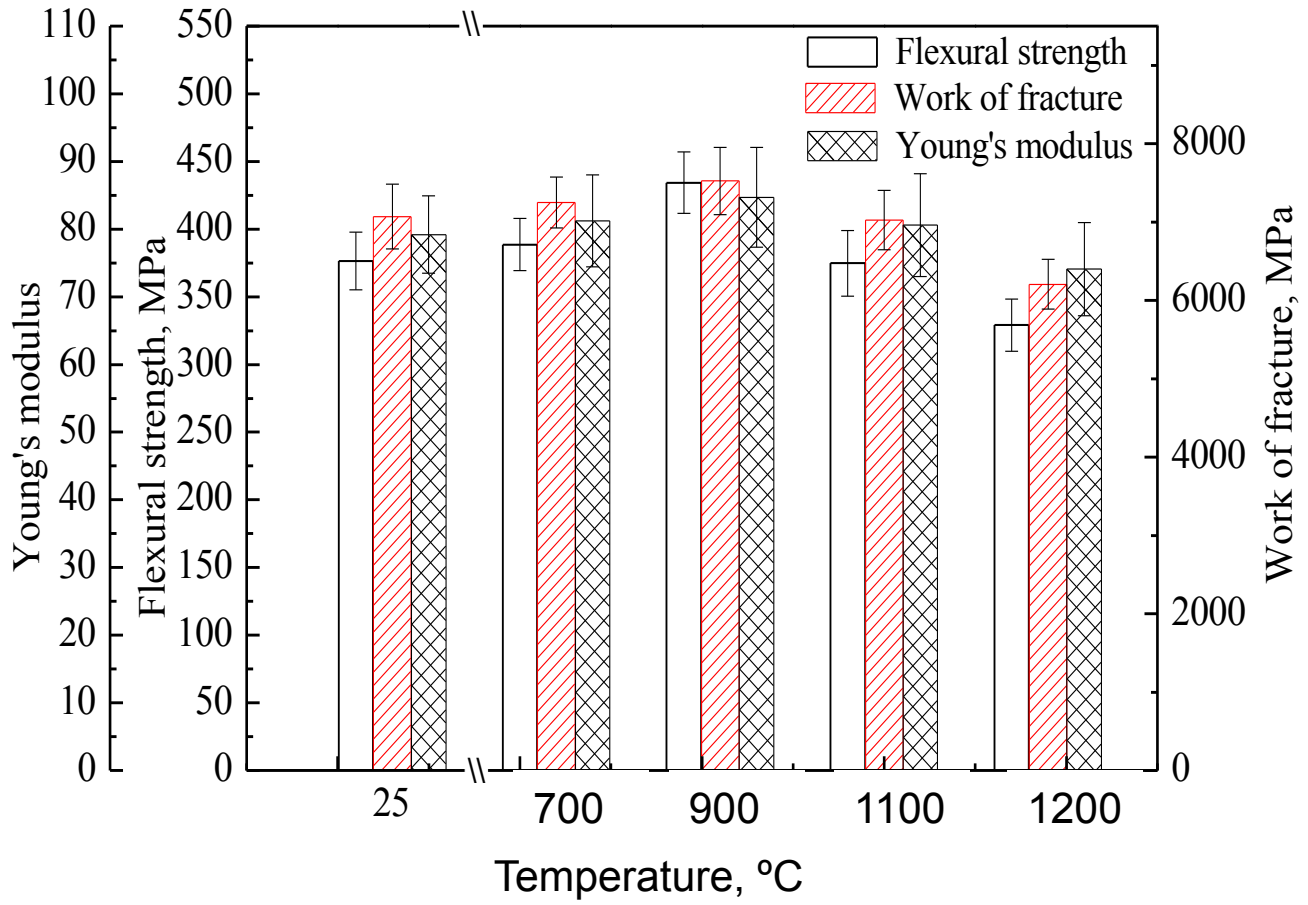

Fig. 4-13 Variation of the elevated temperature mechanical properties of ImHCsKC

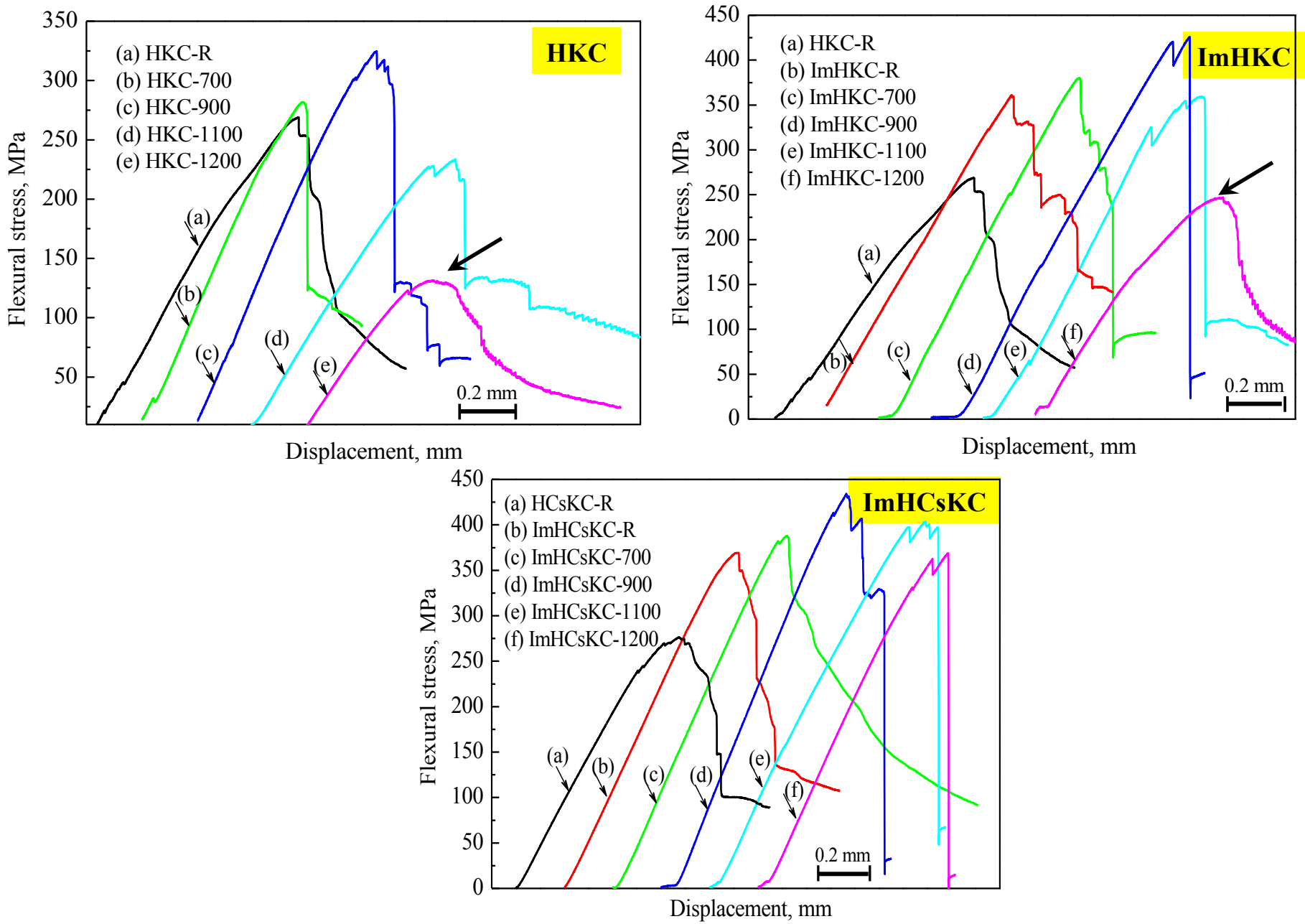

Fig.4-14 Flexural stress-displacemen curves at different temperature

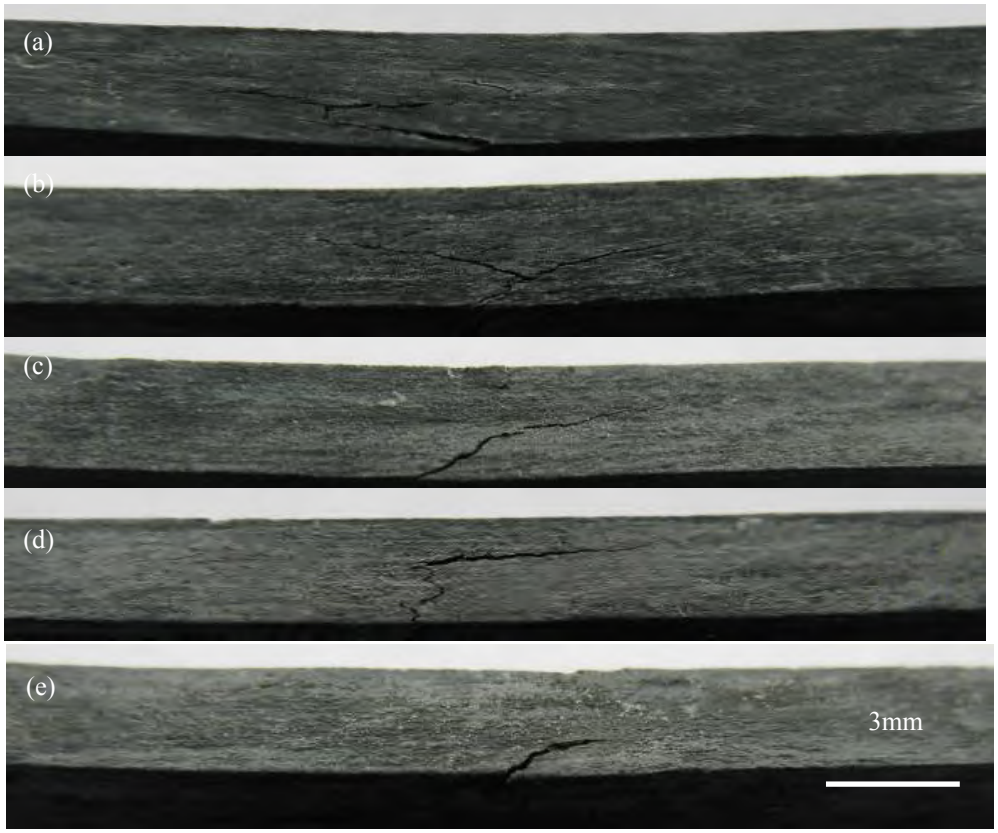

Fig. 4-15 Typical morphologies of ImHC specimens after bending tests at (a) RT, (b) 700℃, (c) 900℃, (d) 1100℃ and (e) 1200℃

---- Peigang He, Dechang Jia. *Journal of the European Ceramic Society*. 2010, 30 (15), 3053–3061.

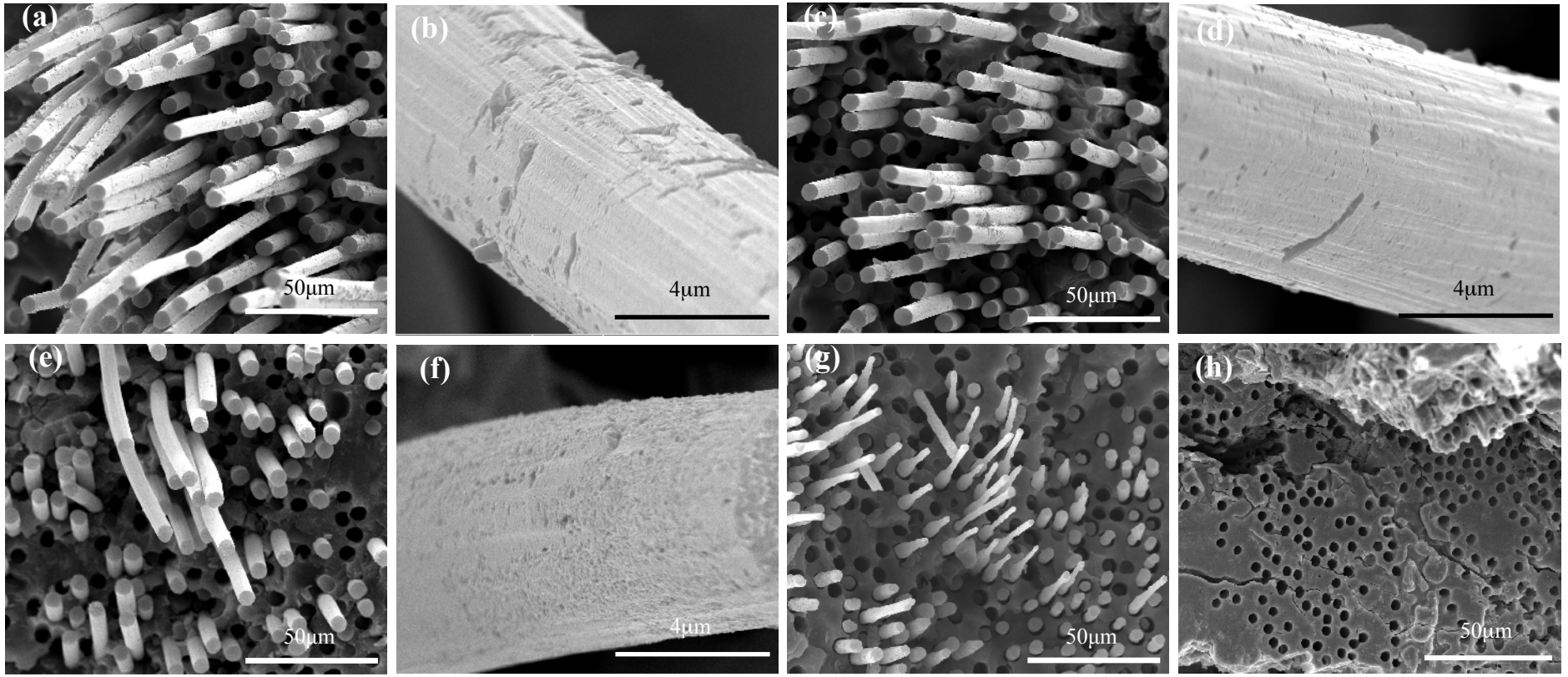

Fig. 4-16 Fractographs near the tensile sides of:
(a), (b) ImHKC-R; (c), (d) ImHKC-700; (e), (f) ImHKC-900; (g) ImHKC-1100; (h) ImHKC-1200

---- Peigang He, Dechang Jia. *Journal of the European Ceramic Society*. 2010, 30 (15), 3053–3061.

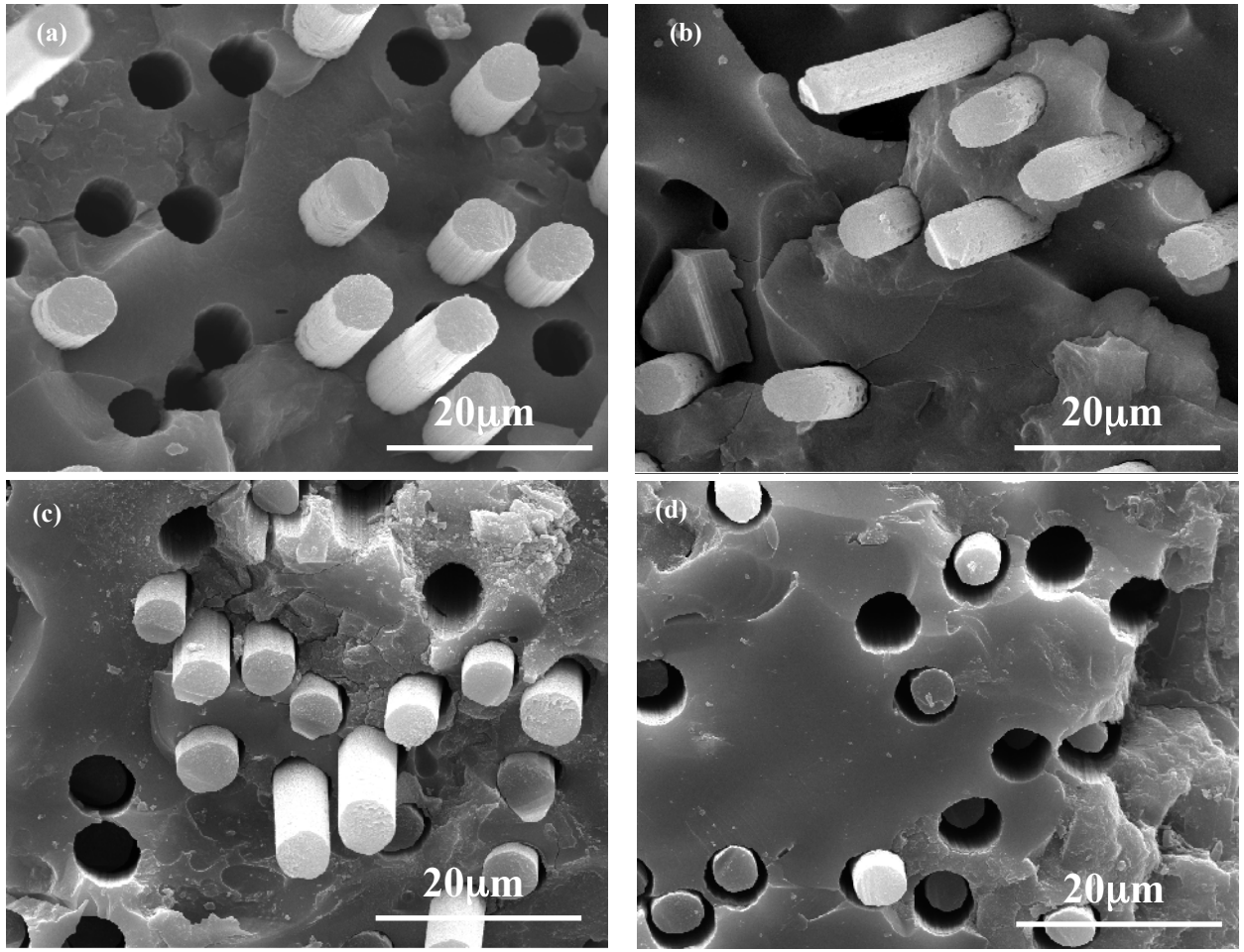

Fig. 4-17 Fractographs obtained at room temperature of ImHC after flexural strength test at: (a) RT, (b) 700℃, (c) 900℃, (d) 1100℃.
Samples were prepared by broking-off the ImHC specimens in cryogenic liquid nitrogen and similar positions were select for observation in each sample

---- Peigang He, Dechang Jia. *Journal of the European Ceramic Society*. 2010, 30 (15), 3053–3061.

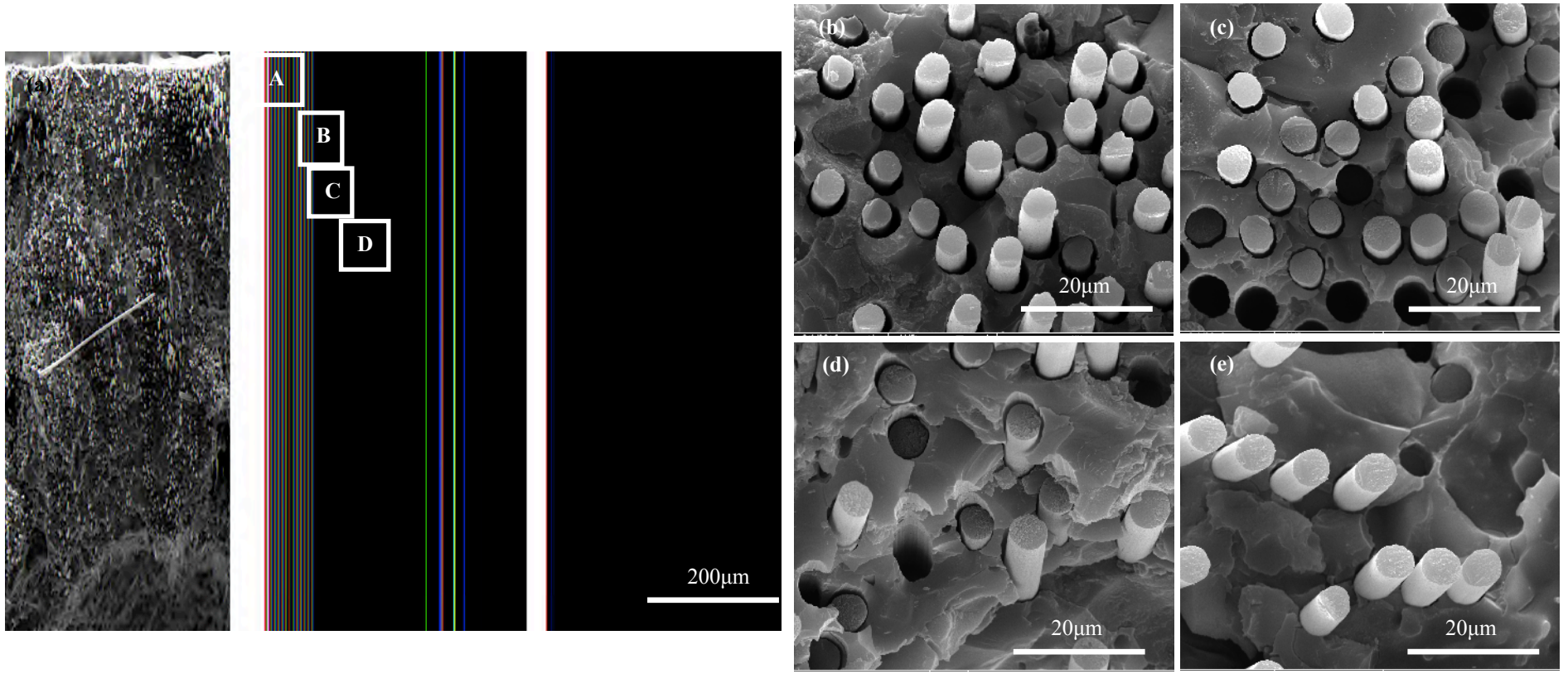

Fig. 4-18 Fractographs obtained at room temperature of ImHC after flexural strength test at 1100: (a) low magnification fractograph, (b)-(e) corresponding to the area of A-D in (a)

$$\text{Degree of Oxidation} = \left(1 - \frac{R_d}{R_0}\right) \times 100\%$$

R_d: Average radius of carbon fiber after test,

R_0: Initial radius of carbon fiber.

---- Peigang He, Dechang Jia. *Journal of the European Ceramic Society*. 2010, 30 (15), 3053–3061.

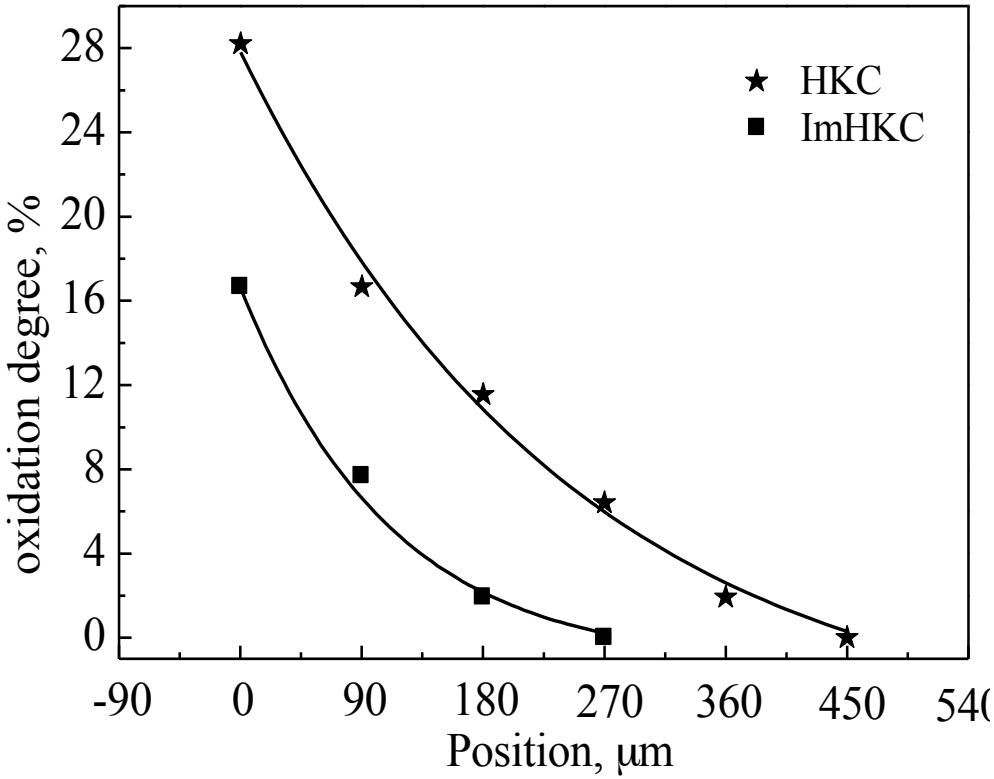

Fig. 4-19 The degree of fiber oxidation vs. distance from the surface of the two composites

---- Peigang He, Dechang Jia. *Journal of the European Ceramic Society*. 2010, 30 (15), 3053–3061.

4.4 Summary

- Repeated sol-SiO_2 impregnation was an efficient method to seal the cracks and pores in the heat-treated composites and thus greatly enhance their relative densities and ambient and high temperature mechanical properties.
- The impregnated composites possess the density of 2.15~2.2g·cm^{-3}, and showed much high specific strength. Composites before & after impregnation fractured in a non-brittle manner at ambient & high temperatures.
- Over an elevated temperature range from 700℃ to 900℃, the strength of the two composites showed anomalous gains and reached their maximum values at 900℃.
- The increased strength was attributed to the cracks blunting and release of residual strength based on the integrity of the carbon fiber.
- Compared with the composites without sol-SiO_2 impregnation, the impregnated one showed superior high temperature properties, which was attributed to the improved fiber integrity due to its much denser microstructure.

5. CONCLUSIONS

① Geopolymer can be converted into ceramic materials heat treated at proper high temperature range. The resulted ceramics possess adjustable coefficient of thermal expansion, which makes them excellent candidate matrix as structural materials.

② With proper heat treatment, carbon fiber reinforced geopolymer composites can be converted into C_f/Leucite composites, which showed excellent high temperature mechanical properties up to 1200°C.

③ Geopolymer technology together with cerium incorporation, high-temperature heat treatment and sol-SiO_2 impregnation etc provides a new method to fabricate a new composites of low cost and high specific strength, which is attractive for elevated temperature applications.


Thanks for your attention!